HHS Public Access

Author manuscript

Cell Rep. Author manuscript; available in PMC 2024 May 17.

Published in final edited form as:

Cell Rep. 2024 April 23; 43(4): 114121. doi:10.1016/j.celrep.2024.114121.

Context-dependent roles for ubiquitous mitochondrial creatine kinase CKMT1 in breast cancer progression

Vinay Ayyappan[1,6], **Nicole M. Jenkinson**[1,6], **Caitlin M. Tressler**[1], **Zheqiong Tan**[1,2], **Menglin Cheng**[1], **Xinyi Elaine Shen**[1], **Alejandro Guerrero**[1], **Kanchan Sonkar**[1], **Ruoqing Cai**[1], **Oluwatobi Adelaja**[1], **Sujayita Roy**[3], **Alan Meeker**[3,4], **Pedram Argani**[3,4], **Kristine Glunde**[1,4,5,7,*]

[1]Johns Hopkins University *In Vivo* Cellular and Molecular Imaging Center, Division of Cancer Imaging Research, Russell H. Morgan Department of Radiology and Radiological Science, Johns Hopkins University School of Medicine, Baltimore, MD, USA

[2]Department of Medical Laboratory, Central Hospital of Wuhan, Tongji Medical College, Huazhong University of Science and Technology, Wuhan, China

[3]Department of Pathology, Johns Hopkins University School of Medicine, Baltimore, MD, USA

[4]Sidney Kimmel Comprehensive Cancer Center, Johns Hopkins University School of Medicine, Baltimore, MD, USA

[5]Department of Biological Chemistry, Johns Hopkins University School of Medicine, Baltimore, MD, USA

[6]These authors contributed equally

[7]Lead contact

SUMMARY

Metabolic reprogramming is a hallmark of cancer, enabling cancer cells to rapidly proliferate, invade, and metastasize. We show that creatine levels in metastatic breast cancer cell lines and secondary metastatic tumors are driven by the ubiquitous mitochondrial creatine kinase (*CKMT1*). We discover that, while *CKMT1* is highly expressed in primary tumors and promotes cell viability, it is downregulated in metastasis. We further show that *CKMT1* downregulation, as seen in breast cancer metastasis, drives up mitochondrial reactive oxygen species (ROS) levels. *CKMT1* downregulation contributes to the migratory and invasive potential of cells by ROS-induced upregulation of adhesion and degradative factors, which can be reversed by antioxidant treatment. Our study thus reconciles conflicting evidence about the roles of metabolites in the

*Correspondence: kglunde@mri.jhu.edu.

AUTHOR CONTRIBUTIONS

Conceptualization—K.G., V.A., and N.M.J.; methodology—V.A., N.M.J., C.M.T., Z.T., M.C., X.E.S., A.G., K.S., R.C., and K.G.; formal analysis—V.A., N.M.J., and K.G.; resources—O.A., S.R., A.M., P.A., and K.G.; writing—V.A., N.M.J., and K.G.; supervision—K.G.; project administration—K.G.; funding acquisition—K.G.

SUPPLEMENTAL INFORMATION

Supplemental information can be found online at https://doi.org/10.1016/j.celrep.2024.114121.

DECLARATION OF INTERESTS

The authors declare no competing interests.

creatine metabolic pathway in breast cancer progression and reveals that tight, context-dependent regulation of *CKMT1* expression facilitates cell viability, cell migration, and cell invasion, which are hallmarks of metastatic spread.

Graphical Abstract

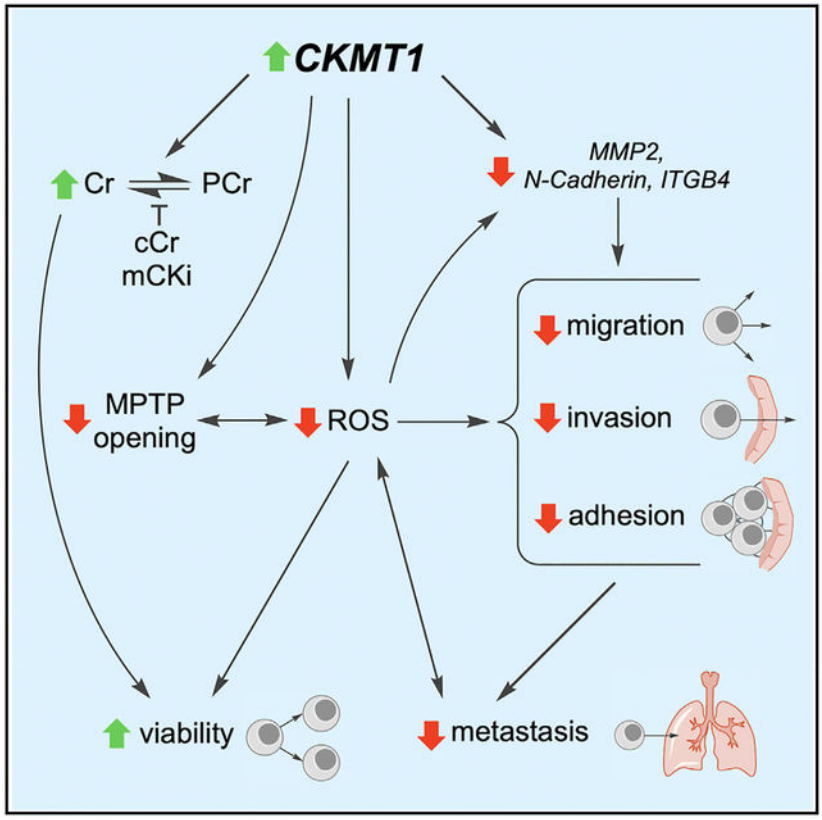

In brief

Ayyappan et al. investigated the role of *CKMT1* in breast cancer progression and showed that *CKMT1* upregulation increases tumor cell growth and viability, while downregulation promotes metastasis. This context-dependent role is tied to *CKMT1*-mediated regulation of the mitochondrial permeability transition pore, which modulates reactive oxygen species release.

INTRODUCTION

Breast cancer is the second most common cancer globally and the most common malignancy among women worldwide.[1,2] Rigorous analysis of breast oncogenesis and tumor progression has uncovered an array of genetic and molecular events and mechanisms associated with primary tumor formation and growth. In particular, altered metabolism, such as of glucose, glutamine, and choline, have been well characterized in the context of their importance to rapid tumor growth in an altered microenvironment.[3–7] However, the bulk of breast cancer mortality is associated with metastatic disease.[2] Due to tremendous intratumoral heterogeneity and an extensive series of changes that accompany the commitment to

initiating metastasis, transcriptional and metabolic profiles of breast cancer metastases can differ substantially from those in the primary tumor.[2] Exploring altered metabolism in breast cancer metastasis at the molecular level may thus open new diagnostic, prognostic, and therapeutic possibilities for patients.

Interest in creatine (Cr) metabolism has increased, as a number of recent reports have described the contribution of Cr and its metabolism to colorectal,[8] blood,[9,10] and subsets of breast cancer.[11] In fact, nutritional Cr supplementation can increase cancer metastasis.[12] However, the involvement of Cr metabolism in breast cancer metastasis has yet to be characterized in detail, as the biological importance of Cr varies across cancers. For example, elevated Cr levels contribute to invasion in pancreatic adenocarcinoma cells[13] and prostate cancer[14] but are seemingly counterproductive to metastatic progression in squamous cell carcinoma.[15] In breast cancer, malignant and metastatic cell lines have been observed to display decreased levels of Cr metabolites,[16] but the mechanism for this trend has yet to be determined in detail. Cells synthesize Cr via a two-step process (Figure 1A). The enzyme L-arginine:glycine amidinotransferase (*AGAT*) first catalyzes the transfer of a guanidinium group from L-arginine to glycine to yield guanidinoacetate, which is methylated by N-guanidinoacetate methyltransferase.[17] Cr kinases reversibly convert the resulting Cr to phosphocreatine (PCr), a process vital to cellular ATP recycling.[18] Linking Cr metabolite profiles associated with malignancy and metastasis to these underlying genetic and molecular factors may thus facilitate the identification of vulnerabilities in breast cancer associated with Cr metabolism and delineate patient populations who may benefit from targeted treatments.

The aim of this study was to identify the molecular causes and functional roles of Cr metabolism in breast cancer metastasis. Using human breast cancer cell lines and patient samples of metastatic and primary breast tumors from the same deceased breast cancer patients, we show that ubiquitous mitochondrial Cr kinase (*CKMT1*) levels are elevated in primary tumors compared to metastases. Further, we illustrate that levels of Cr metabolites are driven by *CKMT1*, which catalyzes Cr-PCr interconversion, contributes to mitochondrial ADP recycling,[19] maintains the mitochondrial inner membrane,[20–23] and is downregulated in metastatic cell lines and metastasized tumors. We finally suggest a context-dependent role of *CKMT1* in breast tumor growth and metastasis whereby *CKMT1* overexpression in the primary tumor decreases reactive oxygen species (ROS) production and promotes increased cell viability. Following *CKMT1* downregulation, increased ROS release then facilitates metastatic capabilities of breast cancer cells.

RESULTS

CKMT1 drives Cr metabolite profiles in human breast cancer cell lines

To investigate the Cr metabolite profile of human breast cancer cells, we performed high-resolution (HR) ^{1}H magnetic resonance spectroscopy (^{1}H MRS) on a panel of six breast cell lines of varying malignancy, aggressiveness, and metastatic potential (Figures 1B and S1A). We observed low total Cr (tCr) levels, which includes Cr and PCr concentrations, in malignant, nonmetastatic (MCF-7), and metastatic breast cancer cell lines (MDA-MB-468, SUM159, and MDA-MB-231) and high tCr in nonmalignant breast epithelial cell lines

(MCF-10A and MCF-12A). While the breast cancer cell line MCF-7 was derived from the cells of a patient with metastatic breast cancer, these cells lack metastatic ability *in vivo* and are neither migratory nor invasive *in vitro*.[24] For this reason, we refer to MCF-7 cells as "malignant, nonmetastatic."

As this initial study pointed toward an overall decrease in Cr metabolism in metastasis, we performed an *in silico* differential expression analysis of a publicly available breast cancer microarray dataset (GSE-69017[25]), wherein mRNA levels were compared from 14 nonmetastatic and 12 metastatic human breast epithelial and breast cancer cell lines (Figures 1C; Table S1). Among the six enzymes and transporters involved in Cr metabolism, *CKMT1* was the only gene with significantly decreased mRNA expression levels in cell lines with metastatic potential versus cell lines without metastatic potential. We also detected *CKMT1* downregulation in a panel of human breast cancer cell lines varying in their metastatic potential, which revealed particularly low mRNA and protein expression levels of *CKMT1* in the metastatic breast cancer cell lines MDA-MB-468, SUM159, and MDA-MB-231 (Figures 1D, 1E, and S1B). Notably, malignant breast cancer cell lines with high metastatic potential, lower Cr and PCr levels, and decreased *CKMT1* expression generally showed lower rates of maximal respiration, decreased spare respiratory capacity, and increased glycolytic capacity (Figures 1F, 1G, and S2). This trend is consistent with a potential role of *CKMT1* in mitochondrial ATP generation.

Constitutive overexpression of *CKMT1* in malignant MDA-MB-231 and SUM159 breast cancer cells consistently resulted in significant increases in Cr and PCr (Figure S3A), further demonstrating that *CKMT1* drives, at least partly, cellular PCr and Cr levels in breast cancer cells. While significant changes in PCr/Cr ratio were not observed in metabolite extracts from both *CKMT1*-overexpressing cell lines, we consistently detected significant increases in intracellular pools of upstream metabolites in the Cr metabolite pathway, including arginine (Figures S3B and S3C).

Notably, levels of arginine correlate strongly ($r > 0.8$) with intracellular Cr concentrations, suggesting that intracellular arginine pools are tied to cellular capacity for Cr synthesis (Figures S3D–S3F). Indeed, cancer cell lines like MDA-MB-231 are argini-nosuccinate synthase 1 deficient and thus depend on arginine import to maintain arginine pools.[26] In looking at the effects of *CKMT1* overexpression, we observed increased intracellular arginine following overexpression (Figure S3C), which would be consistent with this notion. We further found that *CKMT1* overexpression increased the mRNA expression levels of *AGAT*/*GATM*, also contributing to increased tCr-metabolite biosynthesis in these cells.

CKMT1 is upregulated in primary tumors and downregulated in metastases

Prior work in other cancers has suggested that PCr promotes metastatic behavior,[13] a phenomenon that runs counter to our observation of decreased PCr in cancer cell lines with high metastatic potential. In SUM159 breast cancer cells, we observed that addition of exogenous PCr to cell culture media did not impact cell migration or invasion (Figure S4). Thus, we sought to specifically determine the role of *CKMT1* downregulation in metastatic spread and examined *CKMT1*-correlated functional annotations of genes from the Cancer Genome Atlas (TCGA)[27] and Molecular Taxonomy of Breast Cancer International

Consortium (METABRIC)[28] breast cancer patient datasets. Gene sets associated with cell viability had the most positively correlated expression with that of *CKMT1* in breast cancer patients, which was within the top 5% of the TCGA and the top 2% of the METABRIC dataset. We also detected gene sets associated with migration and cell adhesion among the top 1,000 genes whose expression negatively correlated with that of *CKMT1* (Figure 2A; Tables S2, S3, and S4).

To investigate *CKMT1* protein expression in clinical breast cancer metastasis, we studied a patient cohort of 17 terminal breast cancer patients enrolled in our rapid autopsy program using *CKMT1* immunohistochemistry (IHC). Primary breast tumors, lymph node metastases, multiple systemic metastases, and various normal tissue cores from each patient were arranged on single-patient tissue microarrays (TMAs).[29–33] These TMAs are unique because they contain both normal and cancerous tissue from each site of a given patient, allowing for direct comparison within each patient. In total, these 17 single-patient TMAs contained 148 primary tumor core biopsies and 1,399 metastasis core biopsies derived from 49 different organs.[29–33] *CKMT1* IHC of these 17 TMAs revealed that, while lowly expressed in normal breast tissue, *CKMT1* protein expression was significantly higher in primary tumors and significantly downregulated in secondary tumors in various metastatic sites (Figures 2B and 2C). Our analysis of the dataset GSE-120753,[34] which comprises mRNA expression data between matched primary tumor and lung metastases in a patient-derived xenograft model of triple-negative breast cancer, similarly revealed downregulation of *CKMT1* mRNA in lung metastases compared to primary tumors (Figure 2D). An additional mRNA microarray dataset (GSE-26338)[35] also showed significant downregulation of *CKMT1* in metastatic nodules relative to primary tumors (Figure 2E). This dataset did indicate lower *CKMT1* expression in metastases relative to normal breast as well, which may point to post-transcriptional or post-translational mechanisms.

Divergent effects of *CKMT1* on breast cancer cell viability and metastatic abilities

Since our data show that *CKMT1* downregulation occurs in metastasis, we sought to evaluate whether differences in *CKMT1* expression alone could affect key abilities in breast cancer cells that result in cancer progression, including migration, invasion, adhesion, and proliferation. In MDA-MB-231 and SUM159 cells genetically engineered to overexpress *CKMT1*, we observed a marked reduction in cell migration, invasion, and adhesion (Figures 3A–3C and S5A), which was consistent with the *in silico* analysis of TCGA data in Figure 2A and Tables S2, S3, and S4 showing negative correlation of *CKMT1* expression with expression levels of mRNAs/proteins conferring migration and cell adhesion in patients. We consistently observed downregulation of mRNA expression levels associated with both invasion and cell adhesion in both *CKMT1*-overexpressing metastatic breast cancer cell lines, including downregulation of the degradome marker *MMP2*, homophilic adhesion marker *CDH2*, and heterophilic adhesion marker *ITGB4* (Figure S5B). Using a WST-1 cell viability/proliferation assay, we observed that overexpression of *CKMT1* increased cell viability in MDA-MB-231 and SUM159 cells (Figure 3D), along with elevated mRNA expression levels of the cell proliferation marker Ki67 (Figure S5B).

To complement our gain-of-function experiments with loss-of-function studies, we performed small interfering RNA (siRNA) knockdown of *CKMT1* in MCF-7 and MCF-10A cells, which both have high levels of endogenous *CKMT1* expression (Figure 3E) and are malignant and nonmalignant, respectively. While MCF-7 cells are cancer derived, they have low metastatic potential *in vivo*. Following *CKMT1* knockdown, we observed significant invasion in MCF-7 cells, which does not occur in wild-type MCF-7 cells, as well as significantly increased migration (Figure 3F). While treatment with *CKMT1*-targeting siRNA was unable to elicit invasion of MCF-10A cells (which also do not invade at baseline), *CKMT1* knockdown significantly increased MCF-10A cell migration (Figure 3G). Moreover, cells treated with *CKMT1* siRNA displayed increased mRNA and protein expression of various adhesion molecules and markers of migration and invasion, such as *MMP2*, *CDH2* (*N-Cadherin*), and *ITGB4* (Figures 3H and S6). Taken together, these data strongly suggest that low *CKMT1* expression levels are necessary and sufficient to promote migratory and invasive behavior in breast cancer cells.

To further investigate the mechanism by which *CKMT1* expression affects cell viability, exogenous PCr was added to the media of empty-vector MDA-MB-231 and SUM159 cells, which resulted in increases in cell viability similar to those observed in *CKMT1*-overexpressing cells (Figure S7A). No increases in viability were observed when Cr was added to the media of these cells (Figures S7B and S7C). This finding suggests that the role of *CKMT1* in producing PCr via the Cr-PCr shuttle impacts cell viability. However, *CKMT1* knockdown in MCF-7 and MCF-10A cells resulted in a significant decrease in cell viability in both cell lines (Figure 3I), which was not rescued by the addition of exogenous PCr, suggesting that *CKMT1* impacts cell viability through mechanisms other than PCr production as well (Figure S7D). *CKMT1* also functions as a mitochondrial membrane protein that regulates the mitochondrial permeability transition (MPT), which, in turn, permeabilizes the mitochondrial membrane, thereby permitting ROS production and ultimately resulting in cell death.[19,21,36] Accordingly, we showed that the decrease in cell viability in *CKMT1* knockdown cells was rescued by addition of the mitochondrial antioxidant Mito-TEMPO (Figure S7E).

Previous studies have shown that the addition of cyclocreatine (cCr), a Cr analog that competitively inhibits *CKMT1*-mediated Cr-PCr interconversion, causes decreased cell viability.[11,37] However, the same studies also found that cCr has no effect on mitochondrial stability and MPT induction.[11,37] We observed that, while competitive blockade of *CKMT1* by cCr decreased cell viability, cells could be rescued by addition of PCr (Figure S7A). Of the cell lines tested, MCF-7 cells displayed the lowest sensitivity to cCr, with relatively little change in cell viability at 5 mM cCr, a concentration that induced cell death in other cell types. cCr may not be a pure Cr kinase inhibitor, and while off-target effects of cCr administration are possible, the sensitivity of MCF-7 cells to *CKMT1* knockdown but not to cCr suggests that *CKMT1* plays a multifaceted role in cell viability.

We also evaluated the effect of a specific, irreversible *CKMT1* inhibitor, Mito-CKi,[38] in MCF-7 and MCF-10A cells. Mito-CKi administration led to decreased viability in both cell lines (Figure S8). While PCr was unable to rescue either cell line, we observed Cr rescue in MCF-10A cells but not MCF-7 cells. Administration of Mito-CKi did not result in increased

ROS, suggesting that *CKMT1*'s effects on Cr-PCr interconversion and on MPT/ROS release are independent (Figure S9A).

CKMT1 affects mitochondrial ROS and the expression of degradome and adhesion proteins

To further study the role of *CKMT1* in metastatic breast cancer cells, we sought to assess the effects of *CKMT1* knockdown on ROS release, as previous studies have shown that metastatic cells display increased release of ROS.[39,40] Controlled ROS release has also been proposed to contribute to cell motility and metastatic potential.[41,42] We observed that *CKMT1* knockdown in MCF-7 and MCF-10A cells consistently resulted in increased ROS levels in these two cell lines, as measured by DCFDA/H_2DCFDA ROS (2',7'-dichlorofluorescin diacetate) assay, which could be abrogated by treatment with 1 mM of the mitochondrion-targeted antioxidant Mito-TEMPO (Figure 4A). We also observed, in MCF-10A and MCF-7 cells with *CKMT1* knockdown, that concurrent treatment with Mito-TEMPO (1 μM) reversed *CKMT1* knockdown-induced increases in cell migration and, in MCF-7 cells, cell invasion (Figure 4B). Western blot analysis revealed that increases in migration/invasion and adhesion molecules induced by *CKMT1* knockdown could largely be reversed by Mito-TEMPO treatment (Figures 4C and 4D), though the specific molecules affected by *CKMT1* knockdown are cell line specific (Figures 4C, 4D, and S10).

CKMT1 has previously been associated with aberrant cell signaling, albeit in other cancers,[43] and pathways such as the mitogen-activated protein kinase/ERK pathway have been implicated in ROS sensing and metastasis,[29,39,44] with *ERK2* as an established sensor of ROS with effects on tumor growth and metastasis.[45–48] We observed that, following *CKMT1* knockdown, MCF-7 cells consistently increased expression levels of activated (phosphorylated) *ERK* and particularly of activated *ERK2* (Figures 4C and 4D). Mito-TEMPO treatment of these *CKMT1* knockdown MCF-7 cells resulted in a sharp decrease in activated *ERK* levels (Figures 4C and 4D). However, we did not observe this trend in MCF-10A cells (Figure 4D). Taken together, our data show that reduced *CKMT1* expression levels in breast cancer cells drive up mitochondrial ROS levels, which, in turn, prompts increased cell migration and invasion by altering the expression of adhesion and degradative proteins like *N-Cadherin*, *ITGB4*, and *MMP2*.

We sought to determine whether the increased ROS levels observed following *CKMT1* knockdown were a result of changes in MPT activation or whether these were rather a consequence of *CKMT1*'s role in metabolism, contributing to the efficiency of the electron transport chain by facilitating ATP exchange between cytosolic and mitochondrial compartments. To study this, we tested the ability of cyclosporin A, a well-established inhibitor of MPT,[49] to rescue the increased ROS levels induced by *CKMT1* knockdown. We observed that, while cyclosporin A treatment did not significantly change ROS levels in control MCF-10A or MCF-7 cells, cyclosporin A did rescue ROS levels after *CKMT1* knockdown (Figure S9B). These findings support the role of *CKMT1* as a regulator of MPT and subsequent ROS production.

Metabolic consequences of altered *CKMT1* expression

To further investigate the impact of *CKMT1* on metabolism, we also measured the levels of specific metabolites associated with glycolysis, the tricarboxylic acid (TCA) cycle, and oxidative phosphorylation (Figures S11A and S11D). In both MDA-MB-231 and SUM159 *CKMT1*-overexpressing cells, we observed a significant increase in the ratio of metabolites associated with glycolysis (lactate and alanine) to those associated with the TCA cycle and oxidative phosphorylation (glutamate, aspartate, succinate, and fumarate) as compared to empty vector controls (Figures S11B and S11E). Further, we tested the expression levels of genes associated with glycolysis that may accompany *CKMT1* overexpression, including hexokinase-2 (*HK2*), phosphofructokinase-muscle (*PFKM*), lactate dehydrogenase A (*LDHA*), and lactate dehydrogenase B (*LDHB*) using RT-qPCR. In accordance with the increased levels of glycolytic metabolites, we detected significant upregulation of *HK2*, *PFKM*, and *LDHA* in *CKMT1*-overexpressing MDA-MB-231 cells (Figure S11C) and significant upregulation of *PFKM*, *LDHA*, and *LDHB* in *CKMT1*-overexpressing SUM159 cells (Figure S11F) relative to the corresponding empty vector controls.

In addition, total AXP (ATP+ADP+AMP) levels decreased (by 43% in MDA-MB-231 and by 36% in SUM159) following *CKMT1* overexpression (Figure S12), with a large effect size that did not reach significance. AMP levels did not change significantly; however, increased PCr coupled with decreased AXP could suggest increased use of the Cr kinase system. The resulting increase in PCr synthesis may contribute to increased levels of glycolysis-associated metabolites. Notably, we found no significant difference in cellular ROS between *CKMT1*-overexpressing cells and empty vector cells (Figure S9C). However, using ^{1}H HR MRS (Figure S13A), we noted a general decrease of intracellular levels of metabolites with an established mitochondrial antioxidant function, such as NAD(P)H, NAD(P)+, taurine, and glutathione[50] in *CKMT1*-overexpressing cells compared to empty vector cells, though alterations in individual metabolite concentrations among these were not statistically significant (Figure S13B). This suggests that changes in metabolite pools also contribute to the measured ROS signal in the setting of *CKMT1* overexpression.

Surprisingly, when evaluating the effect of *CKMT1* knockdown on cellular ATP generation, we found no marked changes to glycolytic or oxidative flux (Figure S14), suggesting that other modes of compensation may be at play. Testing for expression levels of cytosolic Cr kinases that could compensate, we found that the breast cell lines evaluated expressed the cytosolic Cr kinase isoforms of brain (*CKB*), but we did not detect the expression of the sarcomeric isoform of mitochondrial Cr kinase (*CKMT2*) or muscle Cr kinase (*CKM*) across all cell lines tested. Notably, we detected, in both *CKMT1* overexpression and knockdown, a corresponding up- and downregulation of the cytosolic Cr kinase *CKB* (Figure S15). In the case of overexpression, upregulation of *CKB* could promote increased use of the Cr kinase system and also support cytosolic ATP generation. These observations suggest compensation by cytosolic Cr kinase for perturbed *CKMT1* expression to mitigate discordance in expression of mitochondrial and cytosolic Cr kinases.

DISCUSSION

In this study, we have shown that metastatic breast cancer cells and metastasized breast tumors in patients expressed reduced levels of *CKMT1*, which resulted in decreased intracellular levels of Cr and PCr in metastatic breast cancer cells. In probing the functional role of *CKMT1* in breast cancer, we observed that elevated *CKMT1* expression levels promoted cell viability, while silencing of cellular *CKMT1* expression increased key metastatic abilities of breast cancer cells, including cell migration and cell invasion. These effects occurred through increased mitochondrial ROS, which, in turn, resulted in upregulation of several adhesion molecules and markers of migratory and invasive cell states. Our study thus points to two independent functions of *CKMT1* in cancer: its influence on ATP generation and its role in regulating ROS.

CKMT1 has been demonstrated previously to catalyze the interconversion of Cr and PCr and is thus directly linked to energy homeostasis and cell viability.[17] We observed that overexpressing *CKMT1* promoted breast cancer cell viability, which was corroborated with loss-of-function experiments using siRNA-mediated knockdown. Meanwhile, we also showed that competitive inhibition of Cr-PCr interconversion using cCr or Mito-CKi decreased cell viability, which is in good agreement with a recent study in prostate cancer.[14] While one possibility is that this increase in viability is tied to an increased capacity for ATP generation, our studies paint a more nuanced picture of *CKMT1*'s role in energy metabolism. In the context of *CKMT1* overexpression, we detected increased glycolytic gene expression levels and glycolytic metabolite concentrations in conjunction with increased Cr and PCr levels. This is in agreement with a recent study on gastric cancer.[51] The increased ratio of metabolic products of glycolysis to those of the TCA cycle and oxidative phosphorylation in both engineered *CKMT1*-overexpressing cell lines suggests that elevated *CKMT1* drives overall cellular metabolism toward glycolytic ATP generation. However, we also noted that, following *CKMT1* knockdown, no obvious changes were detectable in patterns of ATP generation. One possibility is that *CKMT1* overexpression results in a tendency to store phosphate in PCr, which could favor a bias toward glycolysis in cell lines stably overexpressing *CKMT1*. We also note that, in both the setting of *CKMT1* overexpression and knockdown, the expression of cytosolic *CKB* increased or decreased, respectively, which could also help to compensate for changes induced by perturbations in *CKMT1* expression.

As a second role for *CKMT1*, the *CKMT1* protein has been shown previously to locate to the mitochondrial membrane, where it functions as negative regulator of the mitochondrial membrane permeability transition pore (MPTP), whose opening can result in the release of ROS and cell death.[19] Consistent with this role, we observed that PCr supplementation was insufficient to counteract the loss of cell viability following *CKMT1* knockdown. We hypothesize that the role of *CKMT1* as gatekeeper of cellular ROS generation accounts for the seemingly disparate roles of *CKMT1* in breast cancer cell growth and metastasis. Accordingly, it has been suggested that the metastatic potential of the triple-negative cell line MDA-MB-231, which we show to have low endogenous *CKMT1* expression, derives from increased MPTP opening.[52] We show that treating *CKMT1* knockdown cells with cyclosporin A, an MPTP inhibitor, resulted in decreased ROS, supporting the theory that

CKMT1 downregulation indeed increases ROS, at least in part, by increasing transient/flickering MPTP opening and vice versa. Moreover, degradative proteins and adhesion markers implicated in metastasis[53–55] can be induced by ROS.[56,57] Here, we show that ROS release following *CKMT1* downregulation promotes cell-line-specific expression of a wide array of molecules associated with migration, invasion, adhesion, and metastasis, which further supports the theory that *CKMT1* downregulation is likely required for breast cancer cells to metastasize. Our data show that, while *CKMT1* downregulation significantly increased ROS, *CKMT1* upregulation did not decrease ROS. While we identified potential compensatory mechanisms responsible for the asymmetric effects of *CKMT1* overexpression and knockdown on ROS, a prior study suggested that *CKMT1* may prevent MPT through multiple avenues, even beyond those mediated by the classical MPT pore complex.[21] Overexpression of *CKMT1* has been reported to render mitochondria of HeLa cells resistant to subsequent depolarization and permeability transition pore opening, but re-expression of *CKMT1* in HeLa cells following depletion failed to rescue cells from depolarization and MPT.[20,58] This could suggest that, regardless of its effect on baseline levels of ROS in cells, *CKMT1* overexpression might also impact metastasis by preventing subsequent ROS release (for example, by p53Ψ-induced MPT or MMP-3/Rac1 signaling),[59–61] and a commitment to metastasis may require *CKMT1* expression to exist below a particular threshold.

The role of ROS in tumorigenesis and metastasis is complex, with metastasizing cancer cells undergoing several changes in redox regulation during metastasis.[62] Clinical recommendations currently exist against the use of antioxidants during chemotherapy and radiation therapy,[63] and it has been speculated that antioxidant proteins, such as *HMOX1*, are critical to tumorigenesis.[42] On the other hand, cancer-associated fibroblasts have been noted to promote cancer progression in response to elevated ROS levels.[64] Other studies have observed decreases in tumor grade and in metastatic burden following targeted alleviation of mitochondrial oxidative stress.[65] A recent report by Cheung et al. describes a model where the protein *TIGAR*, which decreases ROS generation, is upregulated during pancreatic tumor initiation but is subsequently downregulated to promote metastasis.[48] Similarly, the mitochondrially localized nucleoside diphosphate kinase D (NME4) has been shown in HeLa cells to prevent metastasis, with loss of function triggering pro-metastatic signaling alongside increased ROS.[66] We envision a similar role of *CKMT1* in breast cancer, having observed that decreased *CKMT1* expression activates ROS release.

Differential *CKMT1* expression in cancer varies depending on the type of cancer. In prostate cancer[67] and oral squamous cell carcinoma,[15] for example, *CKMT1* downregulation has been linked to tumor progression. However, in other cancers,[68] including hepatocellular carcinoma,[18,69] leukemia,[10] and lymphoma,[9] *CKMT1* overexpression has been linked to tumor growth and worsened clinical outcomes. A recent report by Kurmi et al. describes the potential of competitive inhibition of *CKMT1* by cCr as an effective adjuvant along with chemotherapy in HER2-positive breast cancers.[11] Here, we confirm their observations of increased *CKMT1* expression in primary breast cancers and, for the first time, probe the role of *CKMT1* in breast cancer metastasis. Indeed, we also show that breast cancer cell lines are susceptible to *CKMT1*-targeted interventions, whether by competitive inhibition or by gene knockdown. With regard to *CKMT1* silencing in particular, our evidence relating

CKMT1 to cellular ROS generation complicates this picture, as the success of therapies that target *CKMT1* may be sensitive to tumor type and stage, which may have varying ROS responses. Additional studies *in vivo* of the impact of different treatment schedules of *CKMT1* targeting combined with antioxidant therapies will shed light on possible avenues of clinical translation of our findings.

Part of the value of identifying metabolic dependencies in cancer lies in the potential of using aberrant metabolic profiles as biomarkers of cancer-related processes. We show a very strong correspondence between *CKMT1* expression and levels of Cr metabolites. This raises the possibility of, in the future, using Cr metabolites as a noninvasive surrogate marker of *CKMT1* expression. This may be possible not only for the purpose of monitoring of potential targeted therapy but also for other applications, including drug-induced cardiotoxicity, which has been observed to accompany mitochondrial Cr kinase downregulation.[23,70–74] Future studies should further explore the application of various imaging technologies, such as ^{1}H or ^{31}P MRS, or spectroscopic imaging, or chemical exchange saturation transfer-magnetic resonance imaging,[75] to monitor Cr metabolites *in vivo*.

In conclusion, we have demonstrated that *CKMT1* in breast cancer cells contributes to positively regulating cell proliferation and negatively regulating migration and cell invasion through ROS. Tight control of *CKMT1* may be necessary in breast cancer cells as they disseminate from the primary tumor and form distant metastases. Our mechanistic findings in cell lines and patient samples motivate follow-up studies focused on developing Cr metabolism-based imaging biomarkers to assess breast cancer progression and *CKMT1*, as well as ROS-based treatment strategies for breast cancer.

Limitations of the study

While we have extensively probed the role of *CKMT1* in breast cancer in this work, many lines of questioning remain open. One of the limitations of this work is that these mechanisms have yet to be investigated in an animal model; a human breast tumor xenograft and metastasis study in mice is slated for the future. Although a targeted array of effector proteins was studied, future work would additionally benefit from untargeted high-throughput proteomics and transcriptomics studies of the effects of *CKMT1* expression and knockdown as well as more mechanistic studies of *CKMT1* regulation. While *CKMT1* was studied in isolation, the broader scope of Cr metabolic pathways in breast cancer is of relevance as well. Given the complicated impacts of Cr, PCr, and Cr kinase inhibition on cell viability, with only Cr improving viability and only PCr providing rescue in the setting of Cr kinase inhibition, studies of Cr import and export (e.g., through *SLC6A8*) coupled with isotope tracing studies would be of interest.

STAR★METHODS

RESOURCE AVAILABILITY

Lead contact—Further information and requests for resources and reagents should be directed to and will be fulfilled by the lead contact, Kristine Glunde, Ph.D. (kglunde@mri.jhu.edu).

Materials availability—This study did not generate new unique reagents.

Data and code availability

- The existing, publicly available data analyzed in this paper accession numbers is available from sources listed in the key resources table. All other data reported in this paper will be shared by the lead contact upon request.
- This paper does not report original code.
- Any additional information required to reanalyze the data reported in this paper is available from the lead contact upon request.

EXPERIMENTAL MODEL AND STUDY PARTICIPANT DETAILS

Cell culture—Two immortalized human mammary epithelial cell lines, i.e., MCF-12A (female, ATCC Cat# CRL-10783, RRID:CVCL_3745) and MCF-10A (female, ATCC Cat# CRL-10317, RRID:CVCL_0598), four human breast cancer cell lines, i.e., MCF-7 (female, ATCC Cat# HTB-22, RRID:CVCL_0031), MDA-MB-468 (female, ATCC Cat# HTB-132, RRID:CVCL_0419), SUM159 (female, BioIVT #SUM-159PT, RRID:CVCL_5423), and MDA-MB-231 (female, ATCC Cat# CRM-HTB-26, RRID:CVCL_0062), and HEK293T packaging cells (female, ATCC Cat# CRL-3216, RRID:CVCL_0063) were used in these studies. All cell lines were obtained from the American Type Culture Collection (ATCC, MD, USA), except SUM159 cells, which were obtained from BioIVT. Cells were used for no more than 10 passages after thawing. Cell lines tested negative for mycoplasma using a PCR-based MycoDtect kit (Greiner Bio-One, Monroe, NC) and were authenticated by STR profiling. These procedures are routinely done every six months. MCF-12A and MCF-10A cells were cultured in Dulbecco's Modified Eagle Medium-Ham's F12 (DMEM-F12, Corning) media supplemented with 10% fetal bovine serum (FBS, Sigma Aldrich, St. Louis, MO), 500 ng/mL hydrocortisone, 20 ng/mL epidermal growth factor, 10 ng/mL insulin, and 100 ng/mL cholera toxin. MCF-7 cells were cultured in Eagle's minimum essential medium (MEM, Gibco) with 10% FBS. MDA-MB-468 cells were cultured in DMEM media supplemented with 10% FBS and 1% GlutaMAX (Invitrogen). SUM159 and HEK293T cells were cultured in DMEM media supplemented with 10% FBS. MDA-MB-231 cells were cultured in RPMI-1640 medium (Gibco) supplemented with 10% FBS. All cells were maintained in an incubator with a humidified atmosphere with 5% CO2 at 37°C.

Single-patient TMAs—The single-patient TMAs used in this study were constructed as previously described.[78,79] Briefly, 17 terminal metastatic breast cancer patients, as described in the supplemental information in Table S6, were enrolled in a rapid autopsy program.

Written consent was obtained for each patient. Protocols were approved by the Institutional Review Board and samples were de-identified prior to analysis. 17 single-patient TMAs were assembled using biopsy cores from each patient's archived primary tumor and from normal tissue and multiple metastatic tumor sites obtained at autopsy.[78,79] Each TMA consisted of 99 cores, each measuring 1.4 mm in diameter. To minimize sampling error, 4 to 5 cores per tumor sample were placed on each TMA. In total, these 17 TMAs combined contained 153 control biopsies, 148 primary tumor biopsies, and 1399 metastasis core biopsies derived from 49 different organs, with 8–16 metastatic sites per patient. Analysis of these TMAs is described in detail below.

METHOD DETAILS

In silico analyses—Publicly available mRNA expression data were accessed through the NCBI Gene Expression Omnibus (GEO) accession database. Expression of *AGAT*, *GAMT*, *CKM*, *CKB*, *CKMT1*, *CKMT2*, and *SLC6A8* were queried from GSE-69017, GSE-26338, and GSE120753.[34,35,80] The corresponding heatmaps were generated using the Morpheus platform (https://software.broadinstitute.org/morpheus/index.html). For GSE-120753, a paired t test was performed to compare primary tumor versus metastatic samples for a given mouse across the dataset.

Dual phase extraction and high-resolution ^{1}H MRS—Cells were harvested by trypsinization with 0.25% Trypsin-EDTA Solution (Sigma-Aldrich) and trypan blue was used to stain dead cells. Cell counts were obtained from viable cells only. Water-soluble metabolites were extracted using the dual-phase extraction method (methanol:chloroform:water = 1:1:1) as previously described.[81–84] The aqueous fractions were lyophilized and re-dissolved in D_2O containing 0.24×10^{-6} mol 3-(trimethylsilyl)propionic-2,2,3,3,-d_4 acid (TSP, Sigma-Aldrich) as chemical shift and concentration reference for metabolite quantification. Fully relaxed high-resolution (HR) ^{1}H MRS was performed using a Bruker Avance-III 750 MHz spectrometer equipped with a 5 mm TXI probe. Water-suppressed spectra were acquired using a 1D NOESY pulse sequence with spectral-width 15,495.86 Hz, 64 K data points, relaxation delay 10 s, 64 scans, 8 dummy scans, receiver gain 40.3, and mixing time 80 ms. The signal integrals of the NCH_3 signals of Cr and PCr at ~3.04 parts/million (ppm), as well as other metabolites as indicated in the spectra were determined and normalized to cell number, which was counted prior to extraction. Water soluble metabolites were quantified using TopSpin software (Bruker BioSpin Corp, Billerica, MA). Each experiment was performed in triplicate to account for biological variation.

Total RNA isolation and qRT-PCR—RNA was extracted using the RNAeasy mini kit (Qiagen, Hilden, Germany) according to instructions provided by the manufacturer as described previously.[84] RNA concentration was measured using an Epoch spectrophotometer system (Biotek, Winooski, VT) at its absorption maximum of 260 nm qScript cDNA supermix (Quanta Biosciences, Gaithersburg, MD) was used to synthesize cDNA, for quantitative real-time PCR by SYBR-green supermix (Quanta Biosciences). Biorad CFX384 (Bio-Rad Laboratories, Hercules, CA) was used for thermal cycling. The ΔΔCT method was used to quantify results, with HPRT used as housekeeping gene. Primers

used for these experiments are listed in the supplemental information. Experiments were performed using two technical replicates and four biological replicates.

Protein lysate preparation and Western blotting—Cells were washed with PBS (Mediatech) prior to addition of RIPA buffer (9806, Cell Signaling Technology, Danvers, MA) with protease/phosphatase inhibitor mix (P8340, Sigma-Aldrich). Cells were collected and homogenized by sonication (10 times alternating 1 s pulse/1 s stop). Samples were centrifuged at 13,000 RPM for 20 min at 4°C. Total protein concentration was measured using a BCA Assay (Thermo-Fisher Scientific, Waltham, MA) according to the manufacturer's instructions. Protein was diluted in water and mixed 3:1 with 4x SDS-PAGE loading buffer (Laemmli buffer with β-mercaptoethanol) for a final protein concentration of 2 μg/μL, and this mixture was heated at 95°C for 10 min to denature soluble proteins. Equal amounts (10 μL) were loaded into a PAGE gel for separation via electrophoresis for 50 min at 120 V and transferred to a PVDF membrane (45 min, 100 V). Membranes were blocked with 5% skim milk in PBS (blocking buffer) for 1 h at room temperature before overnight incubation in 4°C with primary antibody. The membrane was then washed three times with PBST followed by incubation for 45 min at room temperature with horseradish peroxidase conjugated secondary antibody, against the species in which the primary antibody was raised, diluted 1:2000 in blocking buffer. The membrane was then washed three times in PBST. Chemiluminescence was detected using a ChemiDoc imaging system (Bio-Rad) following incubation using the SuperSignal West Pico chemiluminescent substrate kit (Thermo-Fisher Scientific) according to the manufacturer's protocol. Antibodies used were: anti-CKMT1 (Santa Cruz Biotechnology Cat# sc-374080, RRID:AB_10917038; 1:50); anti-CKMT1 (Proteintech, Cat# 15346–1-AP, RRID:AB_2081073, 1:1000); anti-MMP2 (Abcam, Cambridge, UK, Cat# ab9779, RRID:AB_10790084; 1:1000); anti-N-Cadherin (Abcam, Cat# ab18203, RRID: AB_444317, 1:100); anti-ITGB4 (Abcam, Cat# ab29042, RRID: AB_870635, 1:1500); anti-MAPK (ERK1/2) (Sigma-Aldrich, Cat# M5670, RRID: AB_477216, 1:100); anti-Phospho-p44/42 MAPK (ERK1/2) (Cell Signaling Technology, Cat# 9101S, RRID: AB_331646, 1:100); anti-β-actin (Cell Signaling Technology, Cat# 3700, RRID:AB_2242334; 1:5000); anti-GAPDH (Abcam, Cat# ab9483, RRID:AB_307273; 1:5000); anti-HSP60 (Abcam, Cat# ab46798, RRID:AB_881444, 1:1000); anti-vinculin (Abcam, Cat# ab129002, RRID:AB_11144129, 1:1000); anti-ITGB3 (CD61) (Santa Cruz Biotechnology, Cat# sc-46655, RRID:AB_627136, 1:100). All uncropped Western blots are shown in Figure S16.

CKMT1 immunohistochemistry of single-patient tissue microarrays from terminal metastatic breast cancer patients—5-μm thick tissue sections were sectioned from each of the TMA blocks and mounted onto microscopy slides. Slides subjected to hematoxylin and eosin (H&E) staining were submerged in ethanol solutions (concentrations in order of 100%, 100%, 96%, 96%, 70%, 70%) for 3 min. They were then washed for 3 min in water before being submerged in hematoxylin for 3 min. After being rinsed with water, slides were submerged for 30 s in eosin. Slides were again washed with water and then submerged in 100% ethanol for 1 min and 100% xylene for 5 min before coverslips were mounted and slides were dried. Each slide was digitally scanned using a Mirax slide scanner (Carl Zeiss AG, Jena, Germany) at 20x magnification. The resulting

H&E images were annotated by a board-certified pathologist (see Figure S17) using CaseViewer (v2.3, 3DHISTECH, Hungary). Pathological characteristics corresponding to each annotation are shown below. Cancerous regions were used for comparison between primary tumor and metastatic sites.

Annotation	Description
Normal	Non-neoplastic, native to the anatomic site
Stroma	Non-neoplastic hematopoietic cells, fibroblasts, and blood vessels native to the anatomic site
Cancer-associated Stroma	Desmoplastic, fibrous, or hyalinized extracellular matrix, fibroblasts, and blood vessels
Cancer	Glandular pattern carcinoma, neoplastic.
Cancer mixed with stroma	Glandular pattern carcinoma, neoplastic tissue alongside desmoplastic, fibrous, or hyalinized extracellular matrix, fibroblasts, and blood vessels
Necrosis	Cell injury

Immunostaining was performed at the Oncology Tissue Services Core of Johns Hopkins University. Immunostaining for CKMT1 was performed on formalin-fixed, paraffin embedded TMA sections. Briefly, following dewaxing and rehydration, slides were immersed in 1% Tween 20, then heat-induced antigen retrieval was performed in a steamer using Antigen Unmasking Buffer (catalog# H-3300, Vector Labs, Newark, CA) for 25 min. Slides were rinsed in PBST, and endogenous peroxidase and phosphatase was blocked (catalog# S2003, Agilent Dako, Santa Clara, CA) and sections were then incubated with primary antibody; anti- CKMT1 (1:200 dilution; catalog# 15346–1-AP, PTGLab, Rosemont, IL) for 45 min at room temperature. The primary antibodies were detected by 30-min incubation with horseradish peroxidase (HRP)-labeled anti-rabbit secondary antibody (catalog# PV6119, Leica Microsystems) followed by detection with 3,3′-Diaminobenzidine (catalog# D4293, Sigma-Aldrich), counterstaining with Mayer's hematoxylin, dehydration, and mounting. Each slide was digitally scanned using an EVOS M5000 Cell Imaging System (Thermo-Fisher Scientific) at 20x magnification. Expression levels were evaluated based on area of tumor cells and staining intensity, as quantified by ImageJ (0–255 scale). Briefly, images of each TMA were converted to 8-bit images. Regions of interest containing tumor cells, as annotated, were assessed using the ImageJ 'Measure' function. Intensities were averaged across tumor-bearing regions within each TMA and then normalized to the average staining intensity calculated for normal breast tissue.

Constitutive CKMT1 overexpression—HEK293T cells were transfected with pLX304-CKMT1 (purchased via the Horizon CCSB-Broad Lentiviral Expression Collection, RRID:Addgene_25890, Watertown, MA) or pLX304-empty vector, along with the ΔR8.2 packaging vector (from Addgene) and vesicular stomatitis virus (VSVG) envelope vector using Lipofectamine 3000 (ThermoFisher Scientific).[76,77] Virions from the HEK293T culture media were concentrated 48 h after transfection. Concentrated lentiviral suspensions were used to transfect MDA-MB-231 and SUM159 cells in the presence of 3 μg/mL polybrene (Sigma-Aldrich). The transfection was repeated three times. Drug selection was performed using blasticidin (5 μg/mL) to isolate successfully transduced cells.

siRNA transfection—Dharmacon (Lafayette, CO) ON-TARGETplus CKMT1 SMARTPool siRNAs (#L-006708-01-0005) were purchased and used for CKMT1 silencing according to manufacturer's instructions. Briefly, cells were plated in 6-well plates at a density of 5×10^5 cells and treated with siRNA at a concentration of 25 nM. As a control, cells were treated with non-targeting siRNA (#D–001210–01, Dharmacon). Effective knockdown of *CKMT1* was assessed using qRT-PCR and Western blotting.

Functional annotation and co-expression analysis—RNA-sequencing data from two transcriptomic datasets: Molecular Taxonomy of Breast Cancer International Consortium (METABRIC) and The Cancer Genome Atlas (TCGA) were evaluated using the co-expression function available via cBioPortal. The top 1000 genes most positively and most negatively co-expressed with *CKMT1* as measured by Pearson's correlation coefficient from each dataset were compared, and functional annotation software DAVID (RRID:SCR_003033)[85,86] was used to perform functional annotation of gene-sets comprised by the overlap between the top values from each dataset, considering a Benjamini-Hochberg adjusted *p*-value <0.05 and a false discovery rate (FDR) < 0.05 as significant.

Cell migration and invasion assays—Cell migration and invasion assays were performed as described previously.[84] Briefly, migration assays were conducted using Corning transwell inserts with 8 μm pores, which were loaded with 100 μL of serum-free medium containing 2.5×10^5 cells. 600 μL of media containing 3% FBS was added to the lower chamber in 24-well plates. After 16 h of incubation, transwell inserts were removed, cells attached to the tops of the inserts were removed using cotton swabs, and cells attached to the bottom of the inserts were fixed with 4% paraformaldehyde (PFA, Santa Cruz Biotechnology). These were then stained with 1% crystal violet before being imaged at 100x using a Nikon TS100 inverted microscope with a charge-coupled device camera (Tokyo, Japan). Cell numbers in 3 different fields of view per transwell insert were counted using ImageJ's cell counter plugin. Invasion assays were performed using the same protocol, however, transwell inserts were coated with 40 μL of Matrigel (Gibco) and incubated for 30 min prior to addition of cells.

Cell adhesion assay—Matrigel-coated (30 μL per well) 96-well plates were coated for 12 h at 4°C. Cells were starved of serum for 8 h prior to being detached with 0.25% trypsin-EDTA solution (Thermo-Fisher Scientific). Cells were then resuspended at 2×10^5 cells/mL in medium with 0.1% BSA (Invitrogen). Cell suspension (100 μL) was added to wells of the Matrigel-coated plate, which was subsequently incubated at 37°C for 20 min. Serum-free media (100 μL) was used to wash off non-adherent cells. Media (100 μL) supplemented with 10% FBS was then added, and cells were incubated at 37°C for 4 h. WST-1 substrate (10 μL) (Sigma-Aldrich) was added to each well and incubated for an additional 2 h. Absorbance was measured at 450 nm using a Beckman Coulter DU 730 UV/Vis Spectrophotometer to quantify adherent cells.

Reactive oxygen species measurement—DCFDA/H2DCFDA (2',7'-dichlorofluorescin diacetate) assay was performed according to manufacturer's instructions (Abcam, #ab113851). Briefly, a cell suspension containing 2.5×10^4 cells in 100 μL complete

media was added to wells of a 96-well plate and incubated at 37°C overnight. For Cyclosporin A recovery assays, cells were incubated for 24 h in media supplemented with Cyclosporin A, 99+% (Thermo Scientific Chemicals, Cat# J63191.06, CAS# 59865-13-3, ethanol vehicle). MCF-7 cells were treated with 10 μM Cyclosporin A, and MCF-10A cells treated with 20 μM Cyclosporin A. Cells were stained with 25 μM DCFDA for 45 min at 37°C before fluorescence was measured at 485/535nm (excitation/emission). Measurements shown in Figures 4A and S9A were taken with an Agilent BioTek Epoch Microplate Spectrophotometer, and measurements shown in Figures S9B and S9C were acquired with a Molecular Devices SpectraMax iD3 Multi-Mode Microplate Reader.

WST-1 cell viability assay—Cell suspension containing 4×10^3 cells in 100 μL complete media were added to wells of a 96-well plate and incubated at 37°C for 4 h. 10 °L of WST-1 substrate (Sigma-Aldrich) was added to each well, and incubation was continued for an additional 3 h. Absorbance was measured at 450 nm using a Beckman Coulter DU 730 UV/Vis Spectrophotometer to quantify adherent cells.

Seahorse analysis—Cell suspension in 100 μL complete media was added to wells of a 96-well cartridge and incubated at37°C 5% CO_2 overnight. To achieve uniform cell density, the number of cells plated was optimized for each cell line: 4×10^4 cells/well MCF-10A or MCF-12A, 3×10^4 cells/well MCF-7, or 1.5×10^4 cells/well MDA-MB-468, SUM159, or MDA-MB-231. After 24 h, media was replaced with 180 μL Seahorse XF RPMI assay medium (media containing 10 mM glucose used for mitochondrial stress test, glucose-free medium used for glycolysis stress test) and incubated at 37°C for 1 h in a non-CO_2 incubator. Glycolysis or mitochondrial stress tests were then performed per the manufacturer's instructions on an Agilent Seahorse XFe24 Analyzer (Agilent, Savage, MD). Briefly, mitochondrial stress tests were performed by acquiring baseline measurements followed by sequential injections of 1 μM oligomycin, 1 μM carbonyl cyanide-4 (trifluoromethoxy) phenylhydrazone (FCCP), and a mixture of 0.5 μM rotenone with 0.5 μM antimycin-A. Glycolysis stress tests wereperformed by obtaining baseline measurements followed by sequential injections of 10 mM glucose, 1 μM oligomycin, and 50 mM 2-deoxyglucose. Three baseline measurements were acquired in 18 min, and each injection was followed by 3 measurements in 18 min. All equipment, compounds, and media were purchased from Agilent. Each experiment had 6 replicate wells per condition, and all experiments were repeated in triplicate. Statistical analysis was performed using two-way ANOVA after normalizing all measurements by cell number.

QUANTIFICATION AND STATISTICAL ANALYSIS

Unless otherwise described, experiments were performed with three biological replicates, with plate-based assays performed with three technical replicates. Data were processed in Microsoft Office Excel (Microsoft). Unpaired two-tailed student's t-test assuming unequal variance was used, and statistically significant results were defined as those with a p-value <0.05. Data are presented as mean ± standard deviation divided by square root of sample size (standard error), unless otherwise indicated. Seahorse data were analyzed using GraphPad Prism, and significance was determined using a two-way ANOVA test.

Supplementary Material

Refer to Web version on PubMed Central for supplementary material.

ACKNOWLEDGMENTS

We would like to acknowledge Ms. Helen Fedor at the Johns Hopkins School of Medicine Oncology Tissue and Imaging Services Shared Resource, where all TMA and IHC experiments were performed. We would like to thank Dr. Piotr Walczak at the University of Maryland for his kind help with slide scanning. We would like to thank Dr. Erika Pearce and Jonathan Curtis for the use of their Agilent Seahorse XFe24 analyzer and reagents. We would like to thank Dr. Sanghee Chin and Dr. Edward Chouchani for their gift of the Mito-CKi reagent. We would also like to acknowledge the National Institutes of Health for grants R01 CA213492, R01 CA213428, and R01 CA264901.

REFERENCES

1. Ferlay J, Soerjomataram I, Dikshit R, Eser S, Mathers C, Rebelo M, Parkin DM, Forman D, and Bray F (2015). Cancer incidence and mortality worldwide: sources, methods and major patterns in GLOBOCAN 2012. Int. J. Cancer 136, E359–E386. 10.1002/ijc.29210. [PubMed: 25220842]
2. Angus L, Smid M, Wilting SM, van Riet J, Van Hoeck A, Nguyen L, Nik-Zainal S, Steenbruggen TG, Tjan-Heijnen VCG, Labots M, et al. (2019). The genomic landscape of metastatic breast cancer highlights changes in mutation and signature frequencies. Nat. Genet 51, 1450–1458. 10.1038/s41588-019-0507-7. [PubMed: 31570896]
3. Vander Heiden MG, Cantley LC, and Thompson CB (2009). Understanding the Warburg effect: the metabolic requirements of cell proliferation. Science 324, 1029–1033. 10.1126/science.1160809. [PubMed: 19460998]
4. Wise DR, and Thompson CB (2010). Glutamine addiction: a new therapeutic target in cancer. Trends Biochem. Sci 35, 427–433. 10.1016/j.tibs.2010.05.003. [PubMed: 20570523]
5. Glunde K, Bhujwalla ZM, and Ronen SM (2011). Choline metabolism in malignant transformation. Nat. Rev. Cancer 11, 835–848. 10.1038/nrc3162. [PubMed: 22089420]
6. Hanahan D, and Weinberg RA (2011). Hallmarks of cancer: the next generation. Cell 144, 646–674. 10.1016/j.cell.2011.02.013. [PubMed: 21376230]
7. Sonkar K, Ayyappan V, Tressler CM, Adelaja O, Cai R, Cheng M, and Glunde K (2019). Focus on the glycerophosphocholine pathway in choline phospholipid metabolism of cancer. NMR Biomed. 32, e4112. 10.1002/nbm.4112. [PubMed: 31184789]
8. Mooney SM, Rajagopalan K, Williams BH, Zeng Y, Christudass CS, Li Y, Yin B, Kulkarni P, and Getzenberg RH (2011). Creatine kinase brain overexpression protects colorectal cells from various metabolic and non-metabolic stresses. J. Cell. Biochem 112, 1066–1075. [PubMed: 21308735]
9. Kornacker M, Schlattner U, Wallimann T, Verneris MR, Negrin RS, Kornacker B, Staratschek-Jox A, Diehl V, and Wolf J (2001). Hodgkin disease-derived cell lines expressing ubiquitous mitochondrial creatine kinase show growth inhibition by cyclocreatine treatment independent of apoptosis. Int. J. Cancer 94, 513–519. 10.1002/ijc.1502. [PubMed: 11745437]
10. Fenouille N, Bassil CF, Ben-Sahra I, Benajiba L, Alexe G, Ramos A, Pikman Y, Conway AS, Burgess MR, Li Q, et al. (2017). The creatine kinase pathway is a metabolic vulnerability in EVI1-positive acute myeloid leukemia. Nat. Med 23, 301–313. 10.1038/nm.4283. [PubMed: 28191887]
11. Kurmi K, Hitosugi S, Yu J, Boakye-Agyeman F, Wiese EK, Larson TR, Dai Q, Machida YJ, Lou Z, Wang L, et al. (2018). Tyrosine Phosphorylation of Mitochondrial Creatine Kinase 1 Enhances a Druggable Tumor Energy Shuttle Pathway. Cell Metabol. 28, 833–847.e8. 10.1016/j.cmet.2018.08.008.
12. Zhang L, Zhu Z, Yan H, Wang W, Wu Z, Zhang F, Zhang Q, Shi G, Du J, Cai H, et al. (2021). Creatine promotes cancer metastasis through activation of Smad2/3. Cell Metabol. 33, 1111–1123.e4. 10.1016/j.cmet.2021.03.009.
13. Papalazarou V, Zhang T, Paul NR, Juin A, Cantini M, Maddocks ODK, Salmeron-Sanchez M, and Machesky LM (2020). The creatine–phosphagen system is mechanoresponsive in pancreatic adenocarcinoma and fuels invasion and metastasis. Nat. Metab 2, 62–80. 10.1038/s42255-019-0159-z. [PubMed: 32694686]

14. Patel R, Ford CA, Rodgers L, Rushworth LK, Fleming J, Mui E, Zhang T, Watson D, Lynch V, Mackay G, et al. (2022). Cyclocreatine Suppresses Creatine Metabolism and Impairs Prostate Cancer Progression. Cancer Res. 82, 2565–2575. 10.1158/0008-5472.CAN-21-1301. [PubMed: 35675421]
15. Onda T, Uzawa K, Endo Y, Bukawa H, Yokoe H, Shibahara T, and Tanzawa H (2006). Ubiquitous mitochondrial creatine kinase downregulated in oral squamous cell carcinoma. Br. J. Cancer 94, 698–709. 10.1038/sj.bjc.6602986. [PubMed: 16479256]
16. Chan KWY, Jiang L, Cheng M, Wijnen JP, Liu G, Huang P, van Zijl PCM, McMahon MT, and Glunde K (2016). CEST-MRI detects metabolite levels altered by breast cancer cell aggressiveness and chemotherapy response. NMR Biomed. 29, 806–816. 10.1002/nbm.3526. [PubMed: 27100284]
17. Wyss M, and Kaddurah-Daouk R (2000). Creatine and creatinine metabolism. Physiol. Rev 80, 1107–1213. 10.1152/physrev.2000.80.3.1107. [PubMed: 10893433]
18. Fan H, Lv P, Mu T, Zhao X, Liu Y, Feng Y, Lv J, Liu M, and Tang H (2018). LncRNA n335586/miR-924/CKMT1A axis contributes to cell migration and invasion in hepatocellular carcinoma cells. Cancer Lett. 429, 89–99. 10.1016/j.canlet.2018.05.010. [PubMed: 29753758]
19. Meyer LE, Machado LB, Santiago APSA, da-Silva WS, De Felice FG, Holub O, Oliveira MF, and Galina A (2006). Mitochondrial Creatine Kinase Activity Prevents Reactive Oxygen Species Generation. J. Biol. Chem 281, 37361–37371. 10.1074/jbc.m604123200. [PubMed: 17028195]
20. Datler C, and Grimm S (2013). Reconstitution of CKMT1 expression fails to rescue cells from mitochondrial membrane potential dissipation: implications for controlling RNAi experiments. Biochim. Biophys. Acta 1833, 2844–2855. 10.1016/j.bbamcr.2013.07.006. [PubMed: 23880370]
21. Datler C, Pazarentzos E, Mahul-Mellier A-L, Chaisaklert W, Hwang M-S, Osborne F, and Grimm S (2014). CKMT1 regulates the mitochondrial permeability transition pore in a process that provides evidence for alternative forms of the complex. J. Cell Sci 127, 1816–1828. 10.1242/jcs.140467. [PubMed: 24522192]
22. Rojo M, Hovius R, Demel RA, Nicolay K, and Wallimann T (1991). Mitochondrial creatine kinase mediates contact formation between mitochondrial membranes. J. Biol. Chem 266, 20290–20295. [PubMed: 1939087]
23. Speer O, Bäck N, Buerklen T, Brdiczka D, Koretsky A, Wallimann T, and Eriksson O (2005). Octameric mitochondrial creatine kinase induces and stabilizes contact sites between the inner and outer membrane. Biochem. J 385, 445–450. 10.1042/BJ20040386. [PubMed: 15294016]
24. Comşa Ş, Cîmpean AM, and Raica M (2015). The Story of MCF-7 Breast Cancer Cell Line: 40 years of Experience in Research. Anticancer Res. 35, 3147–3154. [PubMed: 26026074]
25. Neve RM, Chin K, Fridlyand J, Yeh J, Baehner FL, Fevr T, Clark L, Bayani N, Coppe J-P, Tong F, et al. (2006). A collection of breast cancer cell lines for the study of functionally distinct cancer subtypes. Cancer Cell 10, 515–527. 10.1016/j.ccr.2006.10.008. [PubMed: 17157791]
26. Qiu F, Chen YR, Liu X, Chu CY, Shen LJ, Xu J, Gaur S, Forman HJ, Zhang H, Zheng S, et al. (2014). Arginine starvation impairs mitochondrial respiratory function in ASS1-deficient breast cancer cells. Sci. Signal 7, ra31. 10.1126/scisignal.2004761.
27. Cancer Genome Atlas Network (2012). Comprehensive molecular portraits of human breast tumours. Nature 490, 61–70. 10.1038/nature11412. [PubMed: 23000897]
28. Curtis C, Shah SP, Chin S-F, Turashvili G, Rueda OM, Dunning MJ, Speed D, Lynch AG, Samarajiwa S, Yuan Y, et al. (2012). The genomic and transcriptomic architecture of 2,000 breast tumours reveals novel subgroups. Nature 486, 346–352. 10.1038/nature10983. [PubMed: 22522925]
29. Wu W-S, Wu J-R, and Hu C-T (2008). Signal cross talks for sustained MAPK activation and cell migration: the potential role of reactive oxygen species. Cancer Metastasis Rev. 27, 303–314. 10.1007/s10555-008-9112-4. [PubMed: 18299806]
30. Wu JM, Halushka MK, and Argani P (2010). Intratumoral heterogeneity of HER-2 gene amplification and protein overexpression in breast cancer. Hum. Pathol 41, 914–917. 10.1016/j.humpath.2009.10.022. [PubMed: 20338615]

31. Almendro V, Kim HJ, Cheng Y-K, Gönen M, Itzkovitz S, Argani P, van Oudenaarden A, Sukumar S, Michor F, and Polyak K (2014). Genetic and phenotypic diversity in breast tumor metastases. Cancer Res. 74, 1338–1348. 10.1158/0008-5472.CAN-13-2357-T. [PubMed: 24448237]
32. Avigdor BE, Cimino-Mathews A, DeMarzo AM, Hicks JL, Shin J, Sukumar S, Fetting J, Argani P, Park BH, and Wheelan SJ (2017). Mutational profiles of breast cancer metastases from a rapid autopsy series reveal multiple evolutionary trajectories. JCI Insight 2, e96896. 10.1172/jci.insight.96896. [PubMed: 29263308]
33. Ščupáková K, Adelaja OT, Balluff B, Ayyappan V, Tressler CM, Jenkinson NM, Claes BS, Bowman AP, Cimino-Mathews AM, White MJ, et al. (2021). Clinical importance of high-mannose, fucosylated, and complex N-glycans in breast cancer metastasis. JCI Insight 6, e146945. 10.1172/jci.insight.146945. [PubMed: 34752419]
34. Echeverria GV, Powell E, Seth S, Ge Z, Carugo A, Bristow C, Peoples M, Robinson F, Qiu H, Shao J, et al. (2018). High-resolution clonal mapping of multi-organ metastasis in triple negative breast cancer. Nat. Commun 9, 5079. 10.1038/s41467-018-07406-4. [PubMed: 30498242]
35. Harrell JC, Prat A, Parker JS, Fan C, He X, Carey L, Anders C, Ewend M, and Perou CM (2012). Genomic analysis identifies unique signatures predictive of brain, lung, and liver relapse. Breast Cancer Res. Treat 132, 523–535. 10.1007/s10549-011-1619-7. [PubMed: 21671017]
36. Bonora M, and Pinton P (2014). The mitochondrial permeability transition pore and cancer: molecular mechanisms involved in cell death. Front. Oncol 4, 302. 10.3389/fonc.2014.00302. [PubMed: 25478322]
37. Dolder M, Walzel B, Speer O, Schlattner U, and Wallimann T (2003). Inhibition of the mitochondrial permeability transition by creatine kinase substrates. J. Biol. Chem 278, 17760–17766. 10.1074/jbc.M208705200. [PubMed: 12621025]
38. Darabedian N, Ji W, Fan M, Lin S, Seo HS, Vinogradova EV, Yaron TM, Mills EL, Xiao H, Senkane K, et al. (2023). Depletion of creatine phosphagen energetics with a covalent creatine kinase inhibitor. Nat. Chem. Biol 19, 815–824. 10.1038/s41589-023-01273-x. [PubMed: 36823351]
39. Jiang J, Wang K, Chen Y, Chen H, Nice EC, and Huang C (2017). Redox regulation in tumor cell epithelial–mesenchymal transition: molecular basis and therapeutic strategy. Signal Transduct. Targeted Ther 2, 17036. 10.1038/sigtrans.2017.36.
40. Sarmiento-Salinas FL, Delgado-Magallón A, Montes-Alvarado JB, Ramírez-Ramírez D, Flores-Alonso JC, Cortés-Hernández P, Reyes-Leyva J, Herrera-Camacho I, Anaya-Ruiz M, Pelayo R, et al. (2019). Breast Cancer Subtypes Present a Differential Production of Reactive Oxygen Species (ROS) and Susceptibility to Antioxidant Treatment. Front. Oncol 9, 480. 10.3389/fonc.2019.00480. [PubMed: 31231612]
41. Hurd TR, DeGennaro M, and Lehmann R (2012). Redox regulation of cell migration and adhesion. Trends Cell Biol. 22, 107–115. 10.1016/j.tcb.2011.11.002. [PubMed: 22209517]
42. Perillo B, Di Donato M, Pezone A, Di Zazzo E, Giovannelli P, Galasso G, Castoria G, and Migliaccio A (2020). ROS in cancer therapy: the bright side of the moon. Exp. Mol. Med 52, 192–203. 10.1038/s12276-020-0384-2. [PubMed: 32060354]
43. Benajiba L, Alexe G, Su A, Raffoux E, Soulier J, Hemann MT, Her-mine O, Itzykson R, Stegmaier K, and Puissant A (2019). Creatine kinase pathway inhibition alters GSK3 and WNT signaling in EVI1-positive AML. Leukemia 33, 800–804. 10.1038/s41375-018-0291-x. [PubMed: 30390009]
44. Ciotti S, Iuliano L, Cefalù S, Comelli M, Mavelli I, Di Giorgio E, and Brancolini C (2020). GSK3b is a key regulator of the ROS-dependent necrotic death induced by the quinone DMNQ. Cell Death Dis. 11, 2. 10.1038/s41419-019-2202-0. [PubMed: 31919413]
45. Cagnol S, and Chambard J-C (2010). ERK and cell death: mechanisms of ERK-induced cell death–apoptosis, autophagy and senescence. FEBSJ. 277, 2–21.
46. Shin S, Dimitri CA, Yoon S-O, Dowdle W, and Blenis J (2010). ERK2 but not ERK1 induces epithelial-to-mesenchymal transformation via DEF motif-dependent signaling events. Mol. Cell 38, 114–127. 10.1016/j.molcel.2010.02.020. [PubMed: 20385094]
47. Hong S-K, Wu P-K, and Park J-I (2018). A cellular threshold for active ERK1/2 levels determines Raf/MEK/ERK-mediated growth arrest versus death responses. Cell. Signal 42, 11–20. 10.1016/j.cell-sig.2017.10.001. [PubMed: 28986121]

48. Cheung EC, DeNicola GM, Nixon C, Blyth K, Labuschagne CF, Tuveson DA, and Vousden KH (2020). Dynamic ROS Control by TIGAR Regulates the Initiation and Progression of Pancreatic Cancer. Cancer Cell 37, 168–182.e4. 10.1016/j.ccell.2019.12.012. [PubMed: 31983610]

49. Bernardi P (1996). The permeability transition pore. Control points of a cyclosporin A-sensitive mitochondrial channel involved in cell death. Biochim. Biophys. Acta 1275, 5–9. 10.1016/0005-2728(96)00041-2. [PubMed: 8688451]

50. Mailloux RJ, McBride SL, and Harper M-E (2013). Unearthing the secrets of mitochondrial ROS and glutathione in bioenergetics. Trends Biochem. Sci 38, 592–602. 10.1016/j.tibs.2013.09.001. [PubMed: 24120033]

51. Mi Y, Li Q, Liu B, Wang D, Liu Z, Wang T, Wang Y, Zang Y, Zhou Y, Wen Y, and Ding Y (2023). Ubiquitous mitochondrial creatine kinase promotes the progression of gastric cancer through a JNK-MAPK/JUN/HK2 axis regulated glycolysis. Gastric Cancer 26, 69–81. 10.1007/s10120-022-01340-7. [PubMed: 36114400]

52. Tu Y-F, Kaipparettu BA, Ma Y, and Wong L-JC (2011). Mitochondria of highly metastatic breast cancer cell line MDA-MB-231 exhibits increased autophagic properties. Biochim. Biophys. Acta 1807, 1125–1132. 10.1016/j.bbabio.2011.04.015. [PubMed: 21570379]

53. Hulit J, Suyama K, Chung S, Keren R, Agiostratidou G, Shan W, Dong X, Williams TM, Lisanti MP, Knudsen K, and Hazan RB (2007). N-cadherin signaling potentiates mammary tumor metastasis via enhanced extracellular signal-regulated kinase activation. Cancer Res. 67, 3106–3116. 10.1158/0008-5472.CAN-06-3401. [PubMed: 17409417]

54. Rizwan A, Cheng M, Bhujwalla ZM, Krishnamachary B, Jiang L, and Glunde K (2015). Breast cancer cell adhesome and degradome interact to drive metastasis. npj Breast Cancer 1, 15017. 10.1038/npjbcancer.2015.17. [PubMed: 28721370]

55. Shay G, Lynch CC, and Fingleton B (2015). Moving targets: Emerging roles for MMPs in cancer progression and metastasis. Matrix Biol. 44–46, 200–206. 10.1016/j.matbio.2015.01.019.

56. Sawicki G (2013). Intracellular regulation of matrix metalloproteinase-2 activity: new strategies in treatment and protection of heart subjected to oxidative stress. Sci. Tech. Rep 2013, 130451. 10.1155/2013/130451.

57. Azimi I, Petersen RM, Thompson EW, Roberts-Thomson SJ, and Monteith GR (2017). Hypoxia-induced reactive oxygen species mediate N-cadherin and SERPINE1 expression, EGFR signalling and motility in MDA-MB-468 breast cancer cells. Sci. Rep 7, 15140. 10.1038/s41598-017-15474-7. [PubMed: 29123322]

58. Schubert A, and Grimm S (2004). Cyclophilin D, a component of the permeability transition-pore, is an apoptosis repressor. Cancer Res. 64, 85–93. 10.1158/0008-5472.can-03-0476. [PubMed: 14729611]

59. Kim CH, Jeon HM, Lee SY, Ju MK, Moon JY, Park HG, Yoo M-A, Choi BT, Yook JI, Lim S-C, et al. (2011). Implication of snail in metabolic stress-induced necrosis. PLoS One 6, e18000. 10.1371/journal.pone.0018000. [PubMed: 21448462]

60. Sabharwal SS, and Schumacker PT (2014). Mitochondrial ROS in cancer: initiators, amplifiers or an Achilles' heel? Nat. Rev. Cancer 14, 709–721. 10.1038/nrc3803. [PubMed: 25342630]

61. Senturk S, Yao Z, Camiolo M, Stiles B, Rathod T, Walsh AM, Nemajerova A, Lazzara MJ, Altorki NK, Krainer A, et al. (2014). p53Ψ is a transcriptionally inactive p53 isoform able to reprogram cells toward a metastatic-like state. Proc. Natl. Acad. Sci. USA 111, E3287–E3296. 10.1073/pnas.1321640111. [PubMed: 25074920]

62. Tasdogan A, Ubellacker JM, and Morrison SJ (2021). Redox Regulation in Cancer Cells during Metastasis. Cancer Discov. 11, 2682–2692. 10.1158/2159-8290.CD-21-0558. [PubMed: 34649956]

63. Jung AY, Cai X, Thoene K, Obi N, Jaskulski S, Behrens S, Flesch-Janys D, and Chang-Claude J (2019). Antioxidant supplementation and breast cancer prognosis in postmenopausal women undergoing chemotherapy and radiation therapy. Am. J. Clin. Nutr 109, 69–78. 10.1093/ajcn/nqy223. [PubMed: 30668630]

64. Martinez-Outschoorn UE, Lin Z, Trimmer C, Flomenberg N, Wang C, Pavlides S, Pestell RG, Howell A, Sotgia F, and Lisanti MP (2011). Cancer cells metabolically "fertilize" the tumor microenvironment with hydrogen peroxide, driving the Warburg effect: implications for

PET imaging of human tumors. Cell Cycle 10, 2504–2520. 10.4161/cc.10.15.16585. [PubMed: 21778829]

65. Sotgia F, Martinez-Outschoorn UE, and Lisanti MP (2011). Mitochondrial oxidative stress drives tumor progression and metastasis: should we use antioxidants as a key component of cancer treatment and prevention? BMC Med. 9, 62. 10.1186/1741-7015-9-62. [PubMed: 21605374]
66. Lacombe ML, Lamarche F, De Wever O, Padilla-Benavides T, Carlson A, Khan I, Huna A, Vacher S, Calmel C, Desbourdes C, et al. (2021). The mitochondrially-localized nucleoside diphosphate kinase D (NME4) is a novel metastasis suppressor. BMC Biol. 19, 228. 10.1186/s12915-021-01155-5. [PubMed: 34674701]
67. Pang B, Zhang H, Wang J, Chen W-Z, Li S-H, Shi Q-G, Liang R-X, Xie B-X, Wu R-Q, Qian X-L, et al. (2009). Ubiquitous mitochondrial creatine kinase is overexpressed in the conditioned medium and the extract of LNCaP lineaged androgen independent cell lines and facilitates prostate cancer progression. Prostate 69, 1176–1187. 10.1002/pros.20969. [PubMed: 19415690]
68. Pavón MA, Parreño M, Téllez-Gabriel M, León X, Arroyo-Solera I, López M, Céspedes MV, Casanova I, Gallardo A, López-Pousa A, et al. (2016). CKMT1 and NCOA1 expression as a predictor of clinical outcome in patients with advanced-stage head and neck squamous cell carcinoma. Head Neck 38 (Suppl 1), E1392–E1403. 10.1002/hed.24232. [PubMed: 26516695]
69. Uranbileg B, Enooku K, Soroida Y, Ohkawa R, Kudo Y, Nakagawa H, Tateishi R, Yoshida H, Shinzawa S, Moriya K, et al. (2014). High ubiquitous mitochondrial creatine kinase expression in hepatocellular carcinoma denotes a poor prognosis with highly malignant potential. Int. J. Cancer 134, 2189–2198. 10.1002/ijc.28547. [PubMed: 24174293]
70. Tokarska-Schlattner M, Wallimann T, and Schlattner U (2002). Multiple interference of anthracyclines with mitochondrial creatine kinases: prefer-ential damage of the cardiac isoenzyme and its implications for drug cardiotoxicity. Mol. Pharmacol 61, 516–523. 10.1124/mol.61.3.516. [PubMed: 11854431]
71. Tokarska-Schlattner M, Wallimann T, and Schlattner U (2006). Alterations in myocardial energy metabolism induced by the anti-cancer drug doxorubicin. C. R. Biol 329, 657–668. 10.1016/j.crvi.2005.08.007. [PubMed: 16945832]
72. Tokarska-Schlattner M, Dolder M, Gerber I, Speer O, Wallimann T, and Schlattner U (2007). Reduced creatine-stimulated respiration in doxorubicin challenged mitochondria: particular sensitivity of the heart. Biochim. Biophys. Acta 1767, 1276–1284. 10.1016/j.bba-bio.2007.08.006. [PubMed: 17935690]
73. Pongprot Y, Sittiwangkul R, Charoenkwan P, and Silvilairat S (2012). Use of cardiac markers for monitoring of doxorubixin-induced cardiotoxicity in children with cancer. J. Pediatr. Hematol. Oncol 34, 589–595. 10.1097/MPH.0b013e31826faf44. [PubMed: 23018571]
74. Gupta A, Rohlfsen C, Leppo MK, Chacko VP, Wang Y, Steenbergen C, and Weiss RG (2013). Creatine kinase-overexpression improves myocardial energetics, contractile dysfunction and survival in murine doxorubicin cardiotoxicity. PLoS One 8, e74675. 10.1371/journal.pone.0074675. [PubMed: 24098344]
75. Cai K, Tain R-W, Zhou XJ, Damen FC, Scotti AM, Hariharan H, Poptani H, and Reddy R (2017). Creatine CEST MRI for Differentiating Gliomas with Different Degrees of Aggressiveness. Mol. Imag. Biol 19, 225–232. 10.1007/s11307-016-0995-0.
76. Yang X, Boehm JS, Yang X, Salehi-Ashtiani K, Hao T, Shen Y, Lubonja R, Thomas SR, Alkan O, Bhimdi T, et al. (2011). A public genome-scale lentiviral expression library of human ORFs. Nat. Methods 8, 659–661. 10.1038/nmeth.1638. [PubMed: 21706014]
77. Stewart SA, Dykxhoorn DM, Palliser D, Mizuno H, Yu EY, An DS, Sabatini DM, Chen ISY, Hahn WC, Sharp PA, et al. (2003). Lenti-virus-delivered stable gene silencing by RNAi in primary cells. RNA 9, 493–501. 10.1261/rna.2192803. [PubMed: 12649500]
78. Wu JM, Fackler MJ, Halushka MK, Molavi DW, Taylor ME, Teo WW, Griffin C, Fetting J, Davidson NE, De Marzo AM, et al. (2008). Heterogeneity of breast cancer metastases: comparison of therapeutic target expression and promoter methylation between primary tumors and their multifocal metastases. Clin. Cancer Res 14, 1938–1946. 10.1158/1078-0432.CCR-07-4082. [PubMed: 18381931]

79. Cimino A, Halushka M, Illei P, Wu X, Sukumar S, and Argani P (2010). Epithelial cell adhesion molecule (EpCAM) is overexpressed in breast cancer metastases. Breast Cancer Res. Treat 123, 701–708. 10.1007/s10549-009-0671-z. [PubMed: 20012351]

80. Keri R (2006). Faculty Opinions recommendation of A collection of breast cancer cell lines for the study of functionally distinct cancer subtypes. Faculty Opinions – Post-Publication Peer Review of the Biomedical Literature. 10.3410/f.1057706.509616.

81. Glunde K, Jie C, and Bhujwalla ZM (2004). Molecular causes of the aberrant choline phospholipid metabolism in breast cancer. Cancer Res. 64, 4270–4276. 10.1158/0008-5472.CAN-03-3829. [PubMed: 15205341]

82. Glunde K, Raman V, Mori N, and Bhujwalla ZM (2005). RNA interference-mediated choline kinase suppression in breast cancer cells induces differentiation and reduces proliferation. Cancer Res. 65, 11034–11043. 10.1158/0008-5472.CAN-05-1807. [PubMed: 16322253]

83. Cao MD, Döpkens M, Krishnamachary B, Vesuna F, Gadiya MM, Lønning PE, Bhujwalla ZM, Gribbestad IS, and Glunde K (2012). Glycerophosphodiester phosphodiesterase domain containing 5 (GDPD5) expression correlates with malignant choline phospholipid metabolite profiles in human breast cancer. NMR Biomed. 25, 1033–1042. 10.1002/nbm.2766. [PubMed: 22279038]

84. Cheng M, Rizwan A, Jiang L, Bhujwalla ZM, and Glunde K (2017). Molecular Effects of Doxorubicin on Choline Metabolism in Breast Cancer. Neoplasia 19, 617–627. 10.1016/j.neo.2017.05.004. [PubMed: 28654865]

85. Huang DW, Sherman BT, and Lempicki RA (2009). Systematic and integrative analysis of large gene lists using DAVID bioinformatics resources. Nat. Protoc 4, 44–57. 10.1038/nprot.2008.211. [PubMed: 19131956]

86. Huang DW, Sherman BT, and Lempicki RA (2009). Bioinformatics enrichment tools: paths toward the comprehensive functional analysis of large gene lists. Nucleic Acids Res. 37, 1–13. 10.1093/nar/gkn923. [PubMed: 19033363]

Highlights

- *CKMT1* has context-dependent roles in primary breast tumor growth and metastasis
- *CKMT1* upregulation promotes breast cancer cell viability and primary tumor growth
- *CKMT1* downregulation elevates ROS levels, which increases cell migration and invasion
- *CKMT1* knockdown-induced ROS release upregulates adhesion and degradative factors

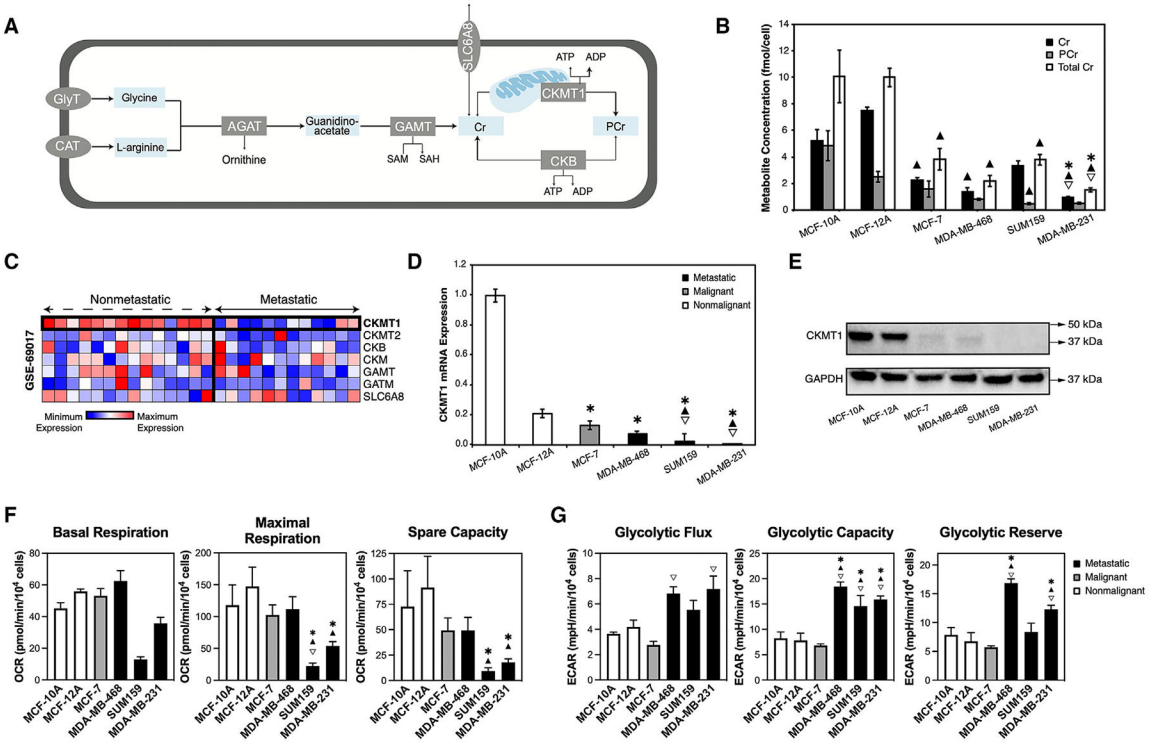

Figure 1. Metastatic breast cancer cells have decreased levels of intracellular Cr metabolites

(A) Schematic describing Cr synthesis and metabolism.

(B) Levels of intracellular Cr, PCr, and tCr (Cr+PCr), as detected by ^{1}H HR MRS in nonmalignant breast epithelial cell lines (MCF-10A and MCF-12A) and breast cancer cell lines of increasing aggressiveness and metastatic potential; $n = 3$ for each cell line. Breast cancer aggressiveness increases from left to right as in MCF-10A, MCF-12A (nonmalignant) < MCF-7 (malignant, nonmetastatic) < MDA-MB-468, SUM159, MDA-MB-231 (metastatic). Significance was determined using a two-tailed t test assuming unequal variance.

(C) Heatmap generated from publicly available microarray dataset GSE69017, which shows the mRNA expression levels of Cr synthesis, transport, and metabolism genes. *CKMT1* expression is downregulated in metastatic compared to nonmetastatic breast cell lines.

(D and E) RT-qPCR (D) and western blot (E) results showing downregulation of *CKMT1* expression in malignant and metastatic breast cancer cell lines; $n = 3$ biological replicates, with 2 technical replicates for RT-qPCR. Significance was determined two-tailed t test assuming unequal variance.

(F) Oxygen consumption rates from the basal respiration, maximal respiration, and spare respiratory capacity phases of the Seahorse mitochondrial stress test, which approximate baseline, maximal, and reserve mitochondrial function.

(G) Extracellular acidification rates from the glycolytic flux, glycolytic capacity, and glycolytic reserve phases of the Seahorse glycolytic stress test, which approximate baseline, maximal, and reserve capacity of glycolysis.

In (F) and (G) $n = 3$ biological replicates, with 6 technical replicates each, and significance was determined using a two-way ANOVA test. For all data, error bars represent standard

error. * denotes $p < 0.05$ with respect to MCF-12A, ▲ denotes $p < 0.05$ with respect to MCF-10A, and ▽ denotes $p < 0.05$ with respect to MCF-7.

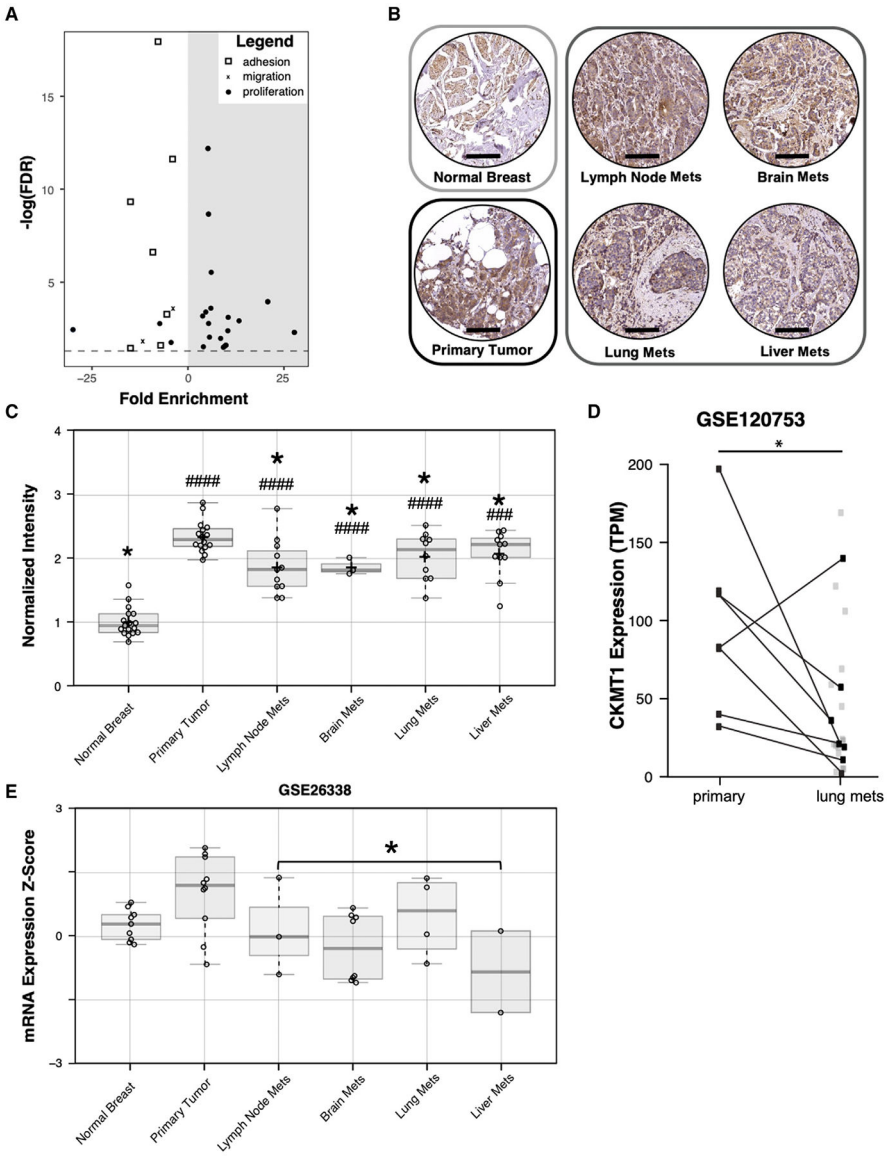

Figure 2. In patients, *CKMT1* is upregulated in primary breast tumors but downregulated in secondary metastasized breast tumors

(A) Volcano plot showing enriched sets of genes co-expressed with *CKMT1* in the TCGA and METABRIC datasets. Significant enrichment was observed for gene sets associated with adhesion and migration among the genes whose expression in patients negatively correlated with expression levels of *CKMT1*. Significant enrichment was also observed for gene sets associated with proliferation among genes whose expression positively correlated with that of *CKMT1*.

(B) Representative microscopic *CKMT1* IHC images showing differences in *CKMT1* levels in normal breast tissue, primary tumors, and lymph node, lung, liver, and brain metastases from the same patient. Scale bars correspond to 100 μm.

(C) Quantification of averaged *CKMT1* staining intensity in primary and metastasized breast tumors from the entire cohort of all 17 patients in this study. Individual data points are averages across TMA cores per tumor site for each of the 17 patients, and box-and-whisker

plots denote mean ± interquartile range (IQR) with the underlying distribution shown. *p < 0.05 compared to primary tumor, ###p < 0.001 compared to normal breast, and ####p < 0.0001 compared to normal breast by a two-tailed t test assuming unequal variance.
(D) Differences in *CKMT1* expression between mouse primary tumor and lung metastases from GSE120753. Black points are connected by a line to represent primary tumor and lung metastasis samples from the same mouse. Additional gray points correspond to additional lung metastasis samples without an associated primary tumor sample from this dataset. *p < 0.05 compared to primary tumor by a two-tailed paired t test.
(E) Z scores of *CKMT1* mRNA expression among normal breast tissue, primary tumors, and lymph node, brain, lung, and liver metastases from GSE-26338. Box-and-whisker plots denote mean ± IQR with the underlying distribution shown. *p < 0.05 compared to primary tumor when all the metastatic sites are grouped by a two-tailed t test.

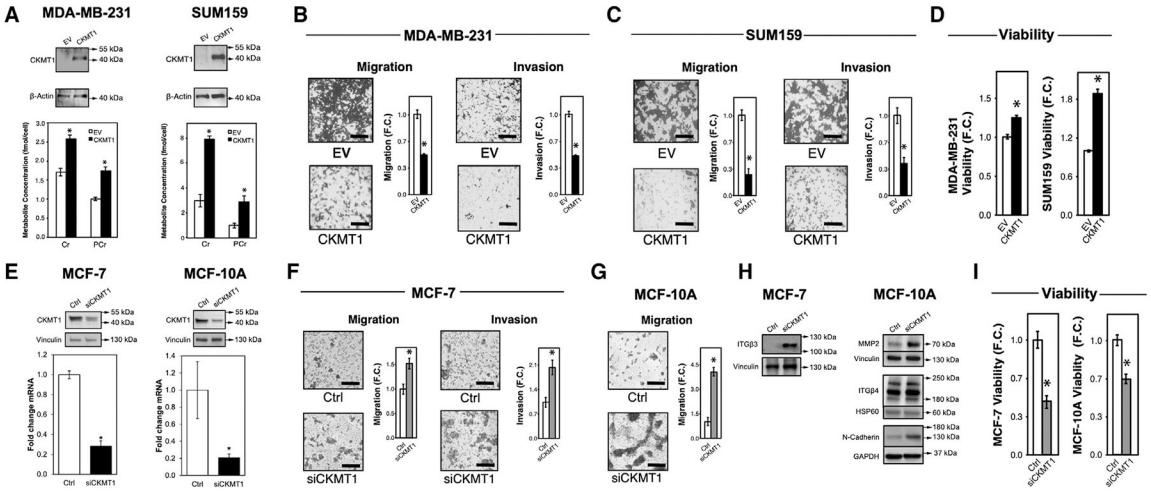

Figure 3. *CKMT1* expression is conducive to proliferation but decreases key metastatic abilities in breast cancer cells

(A) Western blots showing constitutive overexpression of *CKMT1* in MDA-MB-231 and SUM159 cells alongside bar graphs illustrating increased Cr and PCr levels in *CKMT1*-overexpressing (CKMT1) compared to the corresponding empty vector (EV) control cells; $n = 3$.

(B and C) Migration and invasion in (B) MDA-MB-231 cells and (C) SUM159 cells following genetically engineered overexpression of *CKMT1*, showing decreased migration and invasion in *CKMT1*-overexpressing (CKMT1) compared to the corresponding EV cells; $n = 3$. Scale bars correspond to 100 μm.

(D) Viability assay of MDA-MB-231 and SUM159 cells reveals increased cell viability/proliferation of *CKMT1*-overexpressing versus EV cells; $n = 3$ with three technical replicates.

(E) Western blots showing siRNA-mediated knockdown of *CKMT1* in MCF-7 and MCF-10A cells, with bar graphs confirming decreased *CKMT1* mRNA expression in knockdown (siCKMT1) cells compared to the corresponding siRNA control (Ctrl) cells; $n = 3$.

(F and G) Increased migration and invasion in MCF-7 cells (F) and increased migration in MCF-10A cells (G) following *CKMT1* knockdown (siCKMT1). While significant increases in migration were observed in MCF-10A cells, these did not invade at baseline; $n = 3$. Scale bars correspond to 100 μm.

(H) Western blots showing increased expression of the invasion-related proteins *ITGβ3* in MCF-7 cells and *MMP2*, *ITGβ4*, and *N-Cadherin* in MCF-10A cells following CKMT1 knockdown (siCKMT1) compared to the corresponding siRNA control (Ctrl) cells. Western blots are representative of multiple biological replicates; $n = 3$ for ITGβ3, $n = 4$ for N-Cadherin, $n = 5$ for MMP2 and ITGβ4.

(I) Viability assay of MCF-7 and MCF-10A cells shows decreased cell viability/proliferation in *CKMT1* knockdown (siCKMT1) versus the corresponding siRNA control (Ctrl) cells; $n = 3$ with three technical replicates.

*$p < 0.05$ with respect to EV (A–D) or Ctrl (E–I), and significance was determined using a two-tailed t test assuming unequal variance. All bar graphs represent mean + standard error.

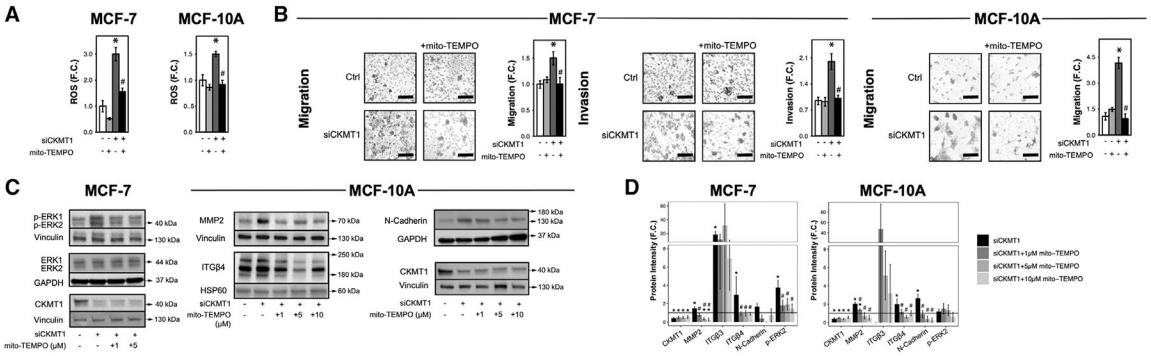

Figure 4. Migration and invasion potentiated by *CKMT1* downregulation depends on mitochondrial reactive oxygen species (ROS) release

(A) Bar graph showing increases in ROS levels (relative to the corresponding siRNA control (Ctrl) cells) in MCF-7 and MCF-10A cells following *CKMT1* knockdown (siCKMT1) as well as decreased ROS levels following treatment with 1 μM of the mitochondrion-specific antioxidant Mito-TEMPO; $n = 3$ with three technical replicates.

(B) Migration and invasion assay results showing that increased migration and invasion following *CKMT1* knockdown are reversed following 1 μM Mito-TEMPO treatment; $n = 3$ for bar graphs presented. Scale bars correspond to 100 μm.

(C) Western blots showing expression of metastasis-related proteins phosphorylated extracellular signal-regulated kinase (*p-ERK)* and *ERK* in MCF-7 and *MMP2*, *ITGβ4*, and *N-Cadherin* in MCF-10A cells following CKMT1 knockdown in the presence and absence of 1, 5, and 10 μM Mito-TEMPO. *MMP2*, *ITGβ4*, and *N-Cadherin* are the same blots that are shown cropped in Figure 3H.

(D) Bar graphs displaying quantified protein levels, normalized to the intensity of the corresponding loading control shown (*GAPDH*, *Vinculin*, or *HSP60*). Data are presented as fold change with respect to Ctrl samples treated with non-targeting siRNA, with error bars representing standard error. Horizontal lines represent y = 1 for Ctrl sample levels.

For (C) and (D), $n = 3$ for *CKMT1* and *ITGβ3*, $n = 4$ for *N-Cadherin*, and $n = 5$ for *MMP2*, *ITGβ4*, and *p-ERK*. $*p < 0.05$ with respect to siControl and $\#p < 0.05$ with respect to siCKMT1 cells without Mito-TEMPO by a two-tailed t test assuming unequal variance.

KEY RESOURCES TABLE

REAGENT or RESOURCE	SOURCE	IDENTIFIER
Antibodies		
anti-CKMTI	Santa Cruz Biotechnology	Cat# sc-374080; RRID:AB_10917038
anti-CKMTI	Proteintech	Cat# 15346-1-AP; RRID:AB_2081073
anti-MMP2	Abcam	Cat# ab9779; RRID:AB_10790084
anti-N-Cadherin	Abcam	Cat# ab18203; RRID: AB_444317
anti-ITGB4	Abcam	Cat# ab29042; RRID: AB_870635
anti-MAPK	Sigma-Aldrich	Cat# M5670; RRID: AB_477216
anti-Phospho-p44/42 MAPK (ERK1/2)	Cell Signaling Technology	Cat# 9101S; RRID: AB_331646
anti-β-actin	Cell Signaling Technology	Cat# 3700; RRID:AB_2242334
anti-GAPDH	Abcam	Cat# ab9483; RRID:AB_307273
anti-HSP60	Abcam	Cat# ab46798; RRID:AB_881444
anti-vinculin	Abcam	Cat# ab129002; RRID:AB_11144129
anti-ITGB3 (CD61)	Santa Cruz Biotechnology	Cat# sc-46655; RRID:AB_627136
(HRP)-labeled anti-rabbit secondary antibody	Cell Signaling Technology	Cat# 7074S; RRID:AB_2099233
(HRP)-labeled anti-mouse secondary antibody	Cell Signaling Technology	Cat# 7076S; RRID:AB_330924
(HRP)-labeled anti-rabbit secondary antibody	Leica Microsystems	Cat# #PV6119; RRID:AB_1307590
Bacterial and virus strains		
E. coli DH5a	Horizon Biosciences	Cat# OHS6085- 213573003
Chemicals, peptides, and recombinant proteins		
Mito-TEMPO	Sigma-Aldrich	Cat# SML0737; CAS# 1334850-99-5
Hydrocortisone	Sigma-Aldrich	Cat# 1316004; CAS #50-23-7
Human insulin, recombinant (yeast)	Roche	Cat# 11376497001; CAS# 11061-68-0
Human epidermal growth factor	Sigma-Aldrich	Cat# E9644; CAS# 62253-63-8
Cholera toxin, Vibrio cholerae, Type Inaba 569B	Sigma-Aldrich	Cat# 227036; CAS# 9012-63-9
Trypsin-EDTA 0.25%	Sigma-Aldrich	Cat# T4049; MDL# MFCD00130286
3-(Trimethylsilyl)propionic-2,2,3,3-d4 acid sodium salt	Sigma-Aldrich	Cat# 269913; CAS# 24493-21-8
2-mercaptoethanol	Gibco	Cat# 21985-023; CAS# 60-24-2
Tween 20	Sigma-Aldrich	Cat# P7949; CAS# 9005-64-5
3,3'-Diaminobenzidine	Sigma-Aldrich	Cat# D4293; CAS# 91-95-2
Paraformaldehyde	Sigma-Aldrich	Cat# P6148; CAS# 30525-89-4
Crystal violet	Sigma-Aldrich	Cat# C0775; CAS# 548-62-9
Bovine serum albumin (BSA)	Sigma-Aldrich	Cat# A7906; CAS# 9048-46-8
Cyclosporin A	Thermo Scientific Chemicals	Cat# J63191.06; CAS #59865-13-3
Mito-CKi (CKi-26)	Mito-CKi was a gift from Edward Chouchani (Darabedian et al.)[38]	N/A
Critical commercial assays		
RNEasy Mini Kit	Qiagen	Cat# 74104
Pierce BCA Assay Kit	ThermoFisher Scientific	Cat# 23227
SuperSignal West Pico chemiluminescent substrate kit	ThermoFisher Scientific	Cat# 34577

REAGENT or RESOURCE	SOURCE	IDENTIFIER
Peroxidase and Alkaline Phosphatase Blocking Reagent	Agilent	Cat# S200389-2
DCFDA/H2DCFDA assay	Abcam	Cat# ab113851
Seahorse XF Cell Mito Stress Test Kit	Agilent	Cat# 103015-100
Seahorse XF Glycolysis Stress Test Kit	Agilent	Cat# 103020-100
Lipofectamine 3000	ThermoFisher Scientific	Cat# L3000001
Deposited data		
METABRIC	cBioPortal	https://www.cbioportal.org/study/summary?id=brca_metabric
RNA sequencing data (TCGA)	The Cancer Genome Atlas	RRID:SCR_003193
Publicly-Available Transcriptomic Datasets	NCBI Gene Expression Omnibus	GSE-69017 GSE-26338 GSE-120753
Experimental models: Cell lines		
MCF-12A	ATCC	Cat# CRL-10783; RRID:CVCL_3745
MCF-10A	ATCC	Cat# CRL-10317; RRID:CVCL_0598
MCF-7	ATCC	Cat# HTB-22; RRID:CVCL_0031
MDA-MB-468	ATCC	Cat# HTB-132; RRID:CVCL_0419
SUM159	BioIVT	Cat# SUM-159PT; RRID:CVCL_5423
MDA-MB-231	ATCC	Cat# CRM-HTB-26; RRID:CVCL_0062
HEK293T	ATCC	Cat# CRL-3216; RRID:CVCL_0063
Oligonucleotides		
ON-TARGETplus CKMT1B SMARTPool siRNAs	Dharmacon	Cat#L-006708-01-0005
siGENOME Non-targeting siRNA #1	Dharmacon	Cat# D-001210-01-05
qRT-PCR primers	Integrated DNA Technologies	See Table S5 in supplemental information for all sequences
Recombinant DNA		
pLX304-CKMT1	Horizon Discovery (Yang et al.)[76]	CCSB-Broad LentiORF - CKMT1B Clone: Cat#OHS6085-213573003; pLX04 backbone: Cat# 25890; RRID:Addgene_25890
pCMV delta R8.2	pCMV delta R8.2 was a gift from Didier Trono	Addgene, Cat# 12263; RRID:Addgene_12263
pCMV-VSV-G	(Stewart at al)[77]	Addgene, Cat# 8454; RRID:Addgene_8454
Software and algorithms		
DAVID	NIH	RRID:SCR_003033
Other		
DMEM/F-12 50/50	Corning	Cat# 15-090-CV
MEM	Gibco	Cat# 11095080
DMEM, high glucose	Gibco	Cat# 11965092
RPMI 1640 medium	Gibco	Cat# 11875119
FBS	Corning	Cat# 35-011-CV
4–15% Mini-PROTEAN TGX Precast Protein Gels	Bio-rad	Cat# 4561083
7.5% Mini-PROTEAN TGX Precast Protein Gels	Bio-rad	Cat# 4561026
6.5 mm transwell, 8.0 μm pore polycarbonate membrane insert	Corning	Cat# 3422
cDNA supermix	Quanta Biosciences	Cat# 95048-025

REAGENT or RESOURCE	SOURCE	IDENTIFIER
SYBR green supermix	Quanta Biosciences	Cat# 95053-500
RIPA buffer	Cell Signaling Technology	Cat# 9806
Protease inhibitor cocktail	Sigma-Aldrich	Cat# P8340; MDL# MFCD00677817
4x Laemmli sample buffer	Bio-Rad	Cat# 1610747
Antigen unmasking buffer	Vector Laboratories	Cat# H-3300-250
Polybrene	Sigma-Aldrich	Cat# TR-1003-G
Matrigel	Corning	Cat# 354234
WST-1	Sigma-Aldrich	Cat# 5015944001